Quaternary Science Reviews
August 2023, Volume 314 Pages 108229 (21p.)
https://doi.org/10.1016/j.quascirev.2023.108229
https://archimer.ifremer.fr/doc/00848/96004/

Dinocyst assemblages and water surface conditions in the Sea of Marmara during MIS 6 and 5 from two long cores

Leroy S.A.G. [1, 2, 3, *], Henry P. [1], Marret F. [3], Pailles C. [1], Licari L. [1], Kende J. [1], Rostek F. [1], Bard E. [1]

[1] Aix Marseille Univ, CNRS, IRD, INRAE, Coll France, CEREGE, Aix-en-Provence, France
[2] Aix Marseille Univ, CNRS, IRD, INRAE, Coll France, CEREGE, Aix-en-Provence, France
[3] School of Environmental Sciences, University of Liverpool, L69 7ZT Liverpool, UK

* Corresponding author : S. A. G. Leroy, email address : suzleroy@hotmail.com

henry@cerege.fr ; fmarret@liverpool.ac.uk ; pailles@cerege.fr ; licari@cerege.fr ; jj.kende@gmail.com ; rostek@cerege.fr ; bard@cerege.fr

Abstract :

The Sea of Marmara is the connection between the vast Black Sea-Caspian Sea basin (Pontocaspian) and the Global Ocean via the Mediterranean Sea. Its water levels and water conditions has widely varied over times. Combining two cores in the Sea of Marmara (Turkey) and using organic-walled dinoflagellate cyst assemblages as the main proxy (combined with alkenones, diatoms and benthic foraminifera), allow qualitatively reconstructing water conditions during Marine Isotopic Stage (MIS) 6 and 5, such as salinity and oxygen level. A clear main marine phase is illustrated in MIS 5e. A minor marine incursion occurred during MIS 5c, mostly supported by alkenone data. The rest of the record indicates brackish Pontocaspian conditions, with more Spiniferites inaequalis in MIS 6 and more S. cruciformis in the non-marine parts of MIS 5.

At the MIS 6/MIS 5 transition, an earlier initial marine flooding in the Sea of Marmara (dinocyst assemblages) in comparison to the Black Sea was highlighted. The marine reconnection occurred at different moments as seen in the terrestrial vegetation reconstructed from pollen analysis linking the two seas.

The sapropels of the Sea of Marmara form when marine water penetrates at depth from the Aegean Sea beneath a layer of lower salinity water. Variations of the residence time of the marine deep water in a stratified Sea of Marmara are potentially an important factor underlying hypoxia/anoxia and sapropel deposition. When combining surface water proxies with benthic foraminifera (test assemblages and presence of inner organic lining), it appears that the successive MIS 5 sapropels formed under decreasing salinity and oxygen availability conditions as the marine inflow was increasingly restricted. Understanding the hydrologic evolution of the Sea of Marmara during MIS 5 implies taking into account that the Bosphorus and Dardanelle straits are hydrodynamically coupled and may not be simplified as on/off switches based on present day sill depths.

Highlights

► Dinocyst analyses of last interglacial and previous glacial in the Sea of Marmara on two long cores. ► Marine phase in MIS5e (dinocysts, benthic foraminifera, alkenones) minor in MIS5c ► BrackishPontocaspian conditions for rest of sequence although different in MIS6 & 5. ► Earlier marine flooding at beginning of MIS5e in Sea of Marmara than in Black Sea. ► Three sapropels highlight decreasing anoxic conditions over time.

Keywords : Dinocysts, MIS 6 and 5, Marmara sea, Connection, Sea level, Sapropel

1 Introduction

The Sea of Marmara (SoM) is a gateway between the Mediterranean Sea and the Black Sea in Turkey. It has experienced water-level fluctuations and hydrological variations during the late Quaternary. They were mainly controlled by bedrock sills at the Marmara Sea exit of Çanakkale (Dardanelles) Strait and the Black Sea entrance of the Istanbul (Bosphorus) Strait. The variations in water depths of these sills were possibly governed by longer-term vertical displacements related to tectonics and erosion/sedimentation balance due to sea-level changes and water exchanges. This occurred not only between the Black and Aegean seas, but also, at a larger scale, between the Ponto-Caspian ensemble and the Global Ocean (Yaltırak, 2002; Gökaşan et al., 2008; Çağatay et al., 2009, 2019; Vidal et al., 2010; Eriş et al., 2011) (Fig. 1). The SoM is indeed a highly seismic area as it is located on the western end of the North Anatolian Fault; however, tectonics are mainly significantly affecting sea levels only in the long term. At the scale of the last climatic cycle, global ocean level change, and thus climate, is the main factor controlling the water level in the SoM. For the last interglacial (Marine Isotope Stage 5, MIS 5), decreasing water level maxima are noted along the successive three warm stages: MIS 5e, 5c and 5a (Rohling et al., 2021). Moreover, the Black Sea level should be considered as another crucial influence on water level in the SoM. Indeed, the melting of the Eurasian icecap and the subsequent evacuation of the freshwater along large rivers flowing into the Black Sea (Soulet et al., 2013; Tudryn et al., 2016) and, at times, the outflow from the Caspian Sea via the Manych Passage (Chepalyga, 2007), affected the amount of water transiting through the SoM. The SoM is the outlet of all the Pontocaspian basins (as far as the Tien-Shan via the Syr-Darya and the Chu River and the Pamir-Indu-Kush via the Amu-Darya). Hence this inland sea is the

receptacle of the history of a large geographical area (Fig. 1). Thus, the water level and water composition history of the SoM is quite complex (local, regional and global forcing) and its insight clearly has an extra-regional relevance. Its history starts to be well-known for the Last Glacial Maximum and the Holocene, but it remains much less clear before (Leroy et al., 2020; Eriş et al., 2007, 2011; Çağatay et al., 2009, 2015a, 2019). Moreover, the SoM forms sapropels under certain conditions (Tolun et al., 2002; Sperling, 2003; Vidal et al., 2010). They are dark and finely laminated sediment rich in organic matter and are important to study as they consist of layers where carbon can be locked away from oxidation, thus contributing to the C cycle. The formation of sapropels is diagnostic of low oxygen availability or absence of oxygen at the seafloor, which has been attributed to deep-water stagnation, enhanced biological production or both. The relative importance of variations of these two factors has been widely debated in the Mediterranean Sea (De Lange et al., 2008; Rohling et al., 2015; Zwiep et al., 2018; and references therein). Oxygen isotope records from planktonic foraminifers and other proxies point to a hydrologic driver: surface water freshening causing water column stratification, thus promoting the development of anoxia in the deep basins, and possibly also influencing productivity (Zwiep et al., 2018; Rohling et al., 2015; Grant et al., 2016; Grimm et al., 2013). In the Sea of Marmara (as in the Black Sea) the water body is not stratified during lacustrine stages (Aloisi et al., 2015) and ingression of seawater is considered as the primary cause of stratification and a requirement for sapropel deposition (Çağatay et al., 2009, 2019). However, at the present day, although the Sea of Marmara has a stable stratification (Beşiktepe et al., 1994), the sediment being deposited is not a sapropel. Somehow a paradox, the Holocene sapropel (MSAP1) in the Sea of Marmara occurred at a time when surface water was inferred to be

more saline than at present, although this sapropel is in large part synchronous with Mediterranean sapropel S1 (Sperling, 2003; Vidal et al., 2010).

Knowledge of the variations of Black Sea salinity beyond the last deglaciation also remains sketchy. Black Sea fauna where dominantly stenohaline during the peak of the Eemian (or equivalently MIS 5e), bottom water was anoxic, and surface salinity probably higher than in the present day (Zubakov, 1988; Shumilovskikh et al., 2013; Wegwerth et al., 2018). Marine incursions may also have occurred during MIS 5a and 5c high stands according to oxygen isotope records obtained on Sofular cave speleothems (Badertscher et al., 2011). These speleothems may reliably inform on the isotopic composition of Black Sea surface waters but are not producing reliable salinity proxies. For instance, during the deglaciation the Black Sea water $\delta^{18}O$ increased from about -10‰ to close to its present-day surface water value (-2.8‰) before reconnection and salinization (Bahr et al., 2006; Soulet et al., 2011).

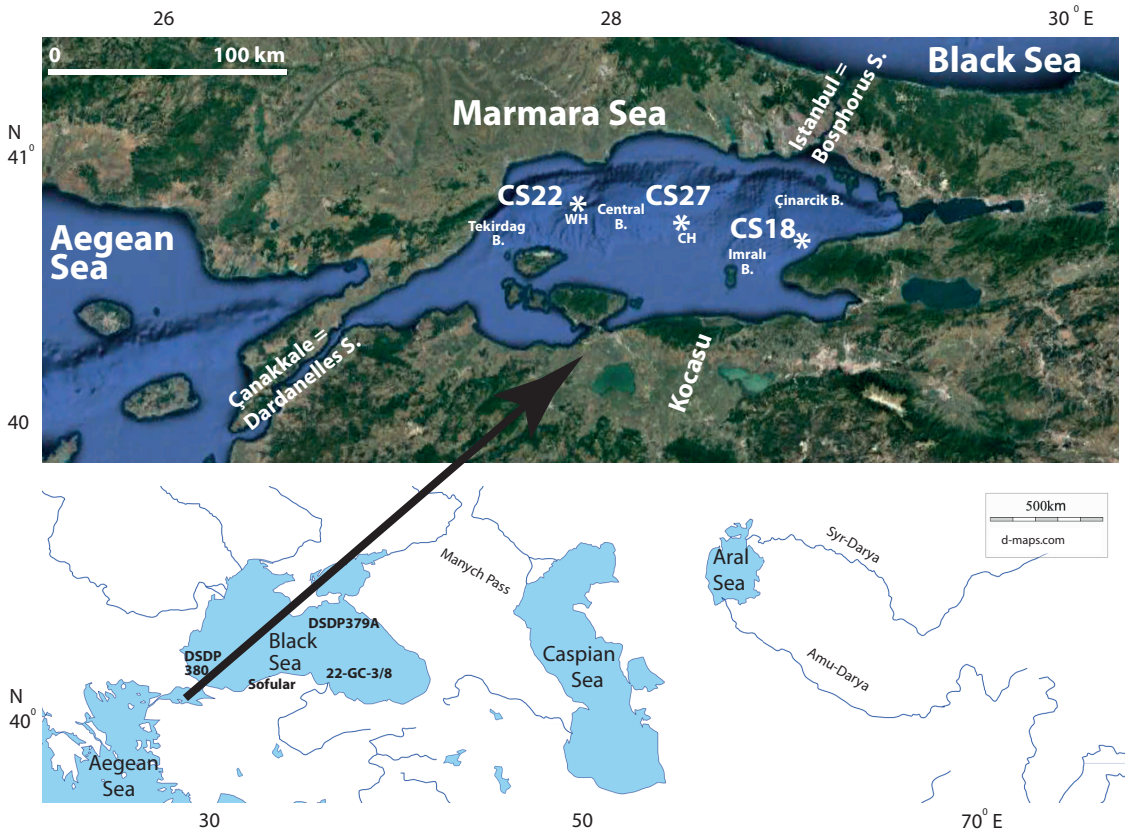

Figure 1: Map of Marmara Sea with core locations (top panel) and map of the seas that were potentially connected at times (lower panel). CH: Central High, WH: Western High, S: Strait, B: Basin. Cores CS22 and CS18 are the focus of this paper.

Owing to a major European research programme, long sediment cores (up to 30 m) were taken in the SoM during the MARSITE cruise (Géli et al., 2014) in 2014 to address some of those key problems (https://cordis.europa.eu/project/id/308417).

The aim of the current investigation is, by using organic-walled dinoflagellate cyst (herein called dinocyst) analysis combined to other proxies such as sedimentary content of C37 alkenone, diatoms and benthic foraminifera, to establish the conditions at the water surface within MIS 5 (130-71 ka ago, Lisiecki and Raymo, 2005) and a large part of MIS 6 (> 130 ka). Thus our results contribute to reconstruct water-level and surface-water-condition history in the SoM. A sister

paper addresses past vegetation, palaeoclimates and chronology on the same samples (Leroy et al., 2023).

2 Regional setting

The SoM (275 km W-E by 80 km N-S) is located at the western end of the North Anatolian Fault where it splits into several strands; as a result, the sea comprises three deep basins (Tekirdag, Central and Çinarcik) separated by two highs: Western High and Central High (Fig. 1). Its deepest location is in the Çınarcık and Central Basins at 1270 m. The water depth of the Dardanelles (Çanakkale) Sill is nowadays 65 m, and that of the Bosphorus (Istanbul) Sill is 35 m (Çağatay et al., 2009). Rivers are mostly inflowing from the south (Kazancı et al., 2004). The Imralı Basin in the SE SoM is nowadays a flat area of a water depth only around 300-400 m (Yaltırak, 2002). The Kocasu (or River Koca), the main river flowing into the SoM, exits now from the continent, south of the Imralı Island. At lower water levels, it has formed deltas prograding into the Imralı Basin and has largely contributed to fill it; later on, the sediment was fed into the Çınarcık Basin along a now-submerged canyon (Kazancı et al., 2004; Sorlien et al., 2012) (Fig. 1). The region immediately around the SoM is relatively flat, although mountains up to 2500 m are found in the S and SE and 1000 m in the N.

Water salinity is 22-24 psu at surface and up to 37-39 psu at depth (Beşiktepe et al., 1994; Aydoğdu et al., 2018). The brackish water of the Black Sea (18 psu), being less dense, outflows through the SoM above the deeper denser Mediterranean saline water moving eastwards (Aydoğdu et al., 2018). The pycnocline is at around 25 m water depth. This delicate two-way setting is easily disturbed by water-level changes leading to deep salinity and oxygenation modifications crucial for the

survival of aquatic ecosystems. Water temperature fluctuates at most from 4 to 28 ºC annually. It displays a slight warming gradient from the NE to the SW: for example, surface water usually varies from 21 (NE) to 26 (SW) ºC in summer. All year round, bottom water is relatively stable at c.15 ºC (Aydoğdu et al., 2018).

The dinocyst assemblages of MIS 6 and 5 have, so far, not been studied in the SoM. However, three dinocyst analyses for these time intervals are available for the Black Sea. In cores DSDP 380 in the SW Black Sea and DSDP Site 379A in the E Black Sea, MIS 5 is covered by a few samples (Ferguson et al., 2018; Hoyle et al., 2021). In the SE Black Sea, a detailed dinocyst diagram of core 22-GC3 includes the period from 129 to 119 ka, with a transition from brackish Pontocaspian to marine conditions at 128 ka (Shumilovskikh et al., 2013) (Fig. 1). More dinocyst records are available for the Late Glacial and Holocene in the SoM (Mudie et al., 2001, 2002, 2004; Londeix et al., 2009) where a change from brackish Pontocaspian to marine conditions was observed at c. 9.5-9 ka. A sapropelic layer, Marmara Sapropel 1 or MSAP-1, was identified at 11.5-7 ka ago (Çağatay et al., 2000; Tolun et al., 2002; Vidal et al., 2010). It is worth mentioning the recent study of dinocyst assemblages on a long core in the Gulf of Corinth, covering the MIS 6 and MIS 5, although further afield, due to the similarity of isolation-connection history of its basin (Fatourou et al., 2023).

3 Previous investigations on cores CS22 and CS18

Calypso cores were taken by the vessel “Pourquoi Pas?” in November 2014. Core MRS-**CS22** (20.42 m long) was obtained close to the top of the Western High at 40,83863 latitude N, 27,79906 longitude E and 551 m water depth (Fig. 1). Core MRS-**CS18** (14.25 m long) was acquired from a slope of the Imralı Basin at

177 40,66206 latitude N and 28,87958 longitude E by 291 m water depth. The core
178 depths of interest are located below a major seismic reflector, i.e. the red-H1
179 reflector (Sorlien et al., 2012; Grall et al., 2013).
180

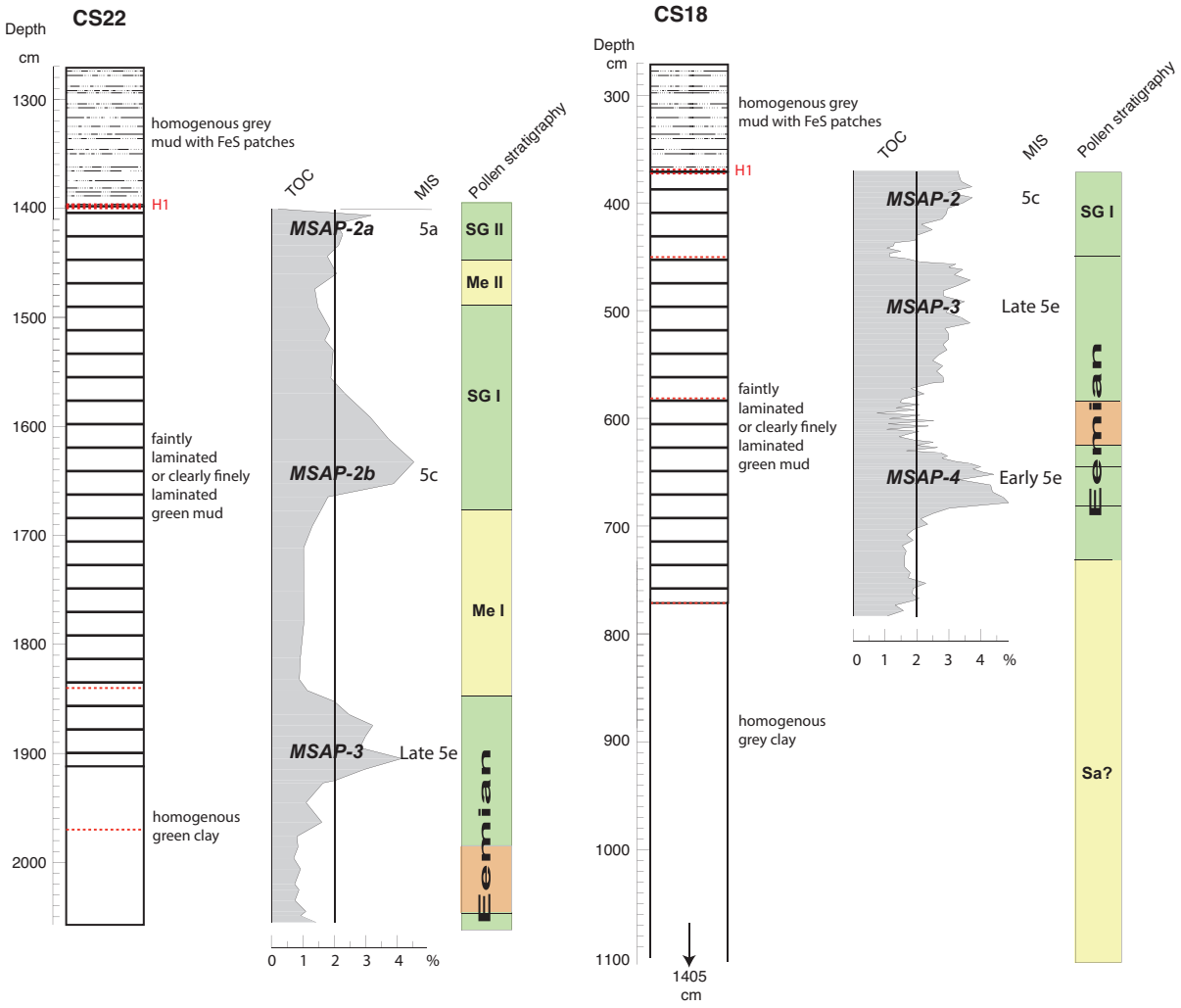

181

182 **Figure 2**: Lithology of cores CS22 and CS18. Hiatus shown as red dotted lines. Total
183 organic carbon in percentage (TOC) with vertical line at 2 % delimiting the sapropels.
184 MIS: Marine Isotopic Stages. Me I = Melisey I Stadial, SG I = Saint-Germain I
185 Interstadial, Me II = Melisey II Stadial, SG II = Saint-Germain II Interstadial, Eem =
186 Eemian Interglacial, according to Leroy et al. (2023).
187

188 Detailed lithological descriptions for cores CS22 and CS18 and the
189 methodology for Total Organic Carbon (TOC) measurements in core CS22 can be
190 found respectively in Kende (2018) and Çağatay et al. (2019). The sediment is a
191 grey or green clay to silty clay at times clearly finely laminated (Fig. 2). In core CS18,
192 only rare benthic foraminifera are present in the 770-700 cm interval, but benthic,
193 with some pelagic foraminifera, become abundant in 700-670 cm and 630-580 cm
194 intervals. However, they are absent in the interval 580-430 cm (Çağatay et al.,
195 2019).

196 Below the red-H1 reflector, the three sapropels (> 2% TOC) were attributed to
197 MIS 5e, 5c and 5a based on correlation of the µ-XRF Ca with the NGRIP $\delta^{18}O$, the
198 TOC correlation with regional pollen records (outside of the SoM), oxygen isotope
199 records in the Mediterranean and global sea level. These are for core CS18: MSAP-
200 4 at 699-623 cm, MSAP-3 at 568-455 cm and MSAP-2 at 430-370 cm depth
201 (sapropel numbering proposed by Çağatay et al., 2009, 2019). These are for core
202 CS22, MSAP-3 at 1920-1853 cm and MSAP-2 in two parts: MSAP-2b at 1653-1570
203 cm and to a lesser extent MSAP-2a at 1460-1407 cm (their naming follows what was
204 proposed in Çağatay et al. (2009)). These authors have proposed a correlation of the
205 MSAP-4, 3 and 2 to the Mediterranean sapropels S5, S4 and S3. A revision of the
206 two Marmara sequence ages, based on geochemistry and pollen analysis, indicates
207 that for core CS22, MSAP-3 is Late Eemian Interglacial, MSAP-2b is Saint-Germain I
208 Interstadial, and MSAP-2a is Saint-Germain II Interstadial, or approximately MIS late
209 5e, 5c and 5a (Fig. 2; Leroy et al., 2023). In core CS18, MSAP-4 is early Eemian
210 Interglacial, MSAP-3 is late Eemian and MSAP-2 is Saint-Germain I, or
211 approximately MIS early 5e, late 5e and 5c (Fig. 2; Leroy et al., 2023).

Minor and major hiati are defined and discussed in Leroy et al. (2023) and shown as red lines on figure 2 and following.

4 Material and Methods

4.1 Dinocyst analysis

Dinoflagellates, a major component of the marine phytoplankton, have a complex life cycle involving a theca that lives in the photic zone and, for about 13 to 16% of the species, an organic-walled cyst is produced in the water column, and settling at the bottom of the sea floor for an obligatory dormancy period (e.g. de Vernal and Marret, 2007; Bravo and Figueroa, 2014; Mudie et al., 2021). Therefore, the distribution of dinocysts in recent sediments has been linked to surface environmental conditions and this relationship has enabled robust quantitative reconstructions of past sea-surface temperature, salinity, productivity and sea-ice cover duration (e.g. de Vernal et al., 2020). A study of 181 surface samples in the Pontocaspian region has clearly highlighted that the dinocyst assemblages reflect surface conditions such as salinity, especially from January to March (Mudie et al., 2017). Fifty-one sediment samples were treated in core CS22 and 79 in core CS18 mostly below the red-H1 reflector for their palynomorph content. The sampling resolution varied between 10 and 20 cm. After measurement of the sediment volume (between 0.5 and 2.5 ml), one tablet of *Lycopodium clavatum* was added. The sediment was then soaked in tetrasodium pyrophosphate, followed by acid attacks: cold HCl (10% dilution), cold HF (between 40 and 60%) and again cold HCl. Samples were then rinsed with distilled water and sieved on nylon meshes at 125 and 10 µm. The residues were transferred to vials and slides mounted in glycerol. At least 60 dinocysts were counted in each sample, except in core CS22 above 1400

cm (24 to 1124 dinocysts), and in core CS18 above 369 cm (39 to 90 dinocysts) and below 786.5 cm (22 to 274 dinocysts). The sums are given in the diagrams. Some gritty samples in core CS18 were also centrifuged in Sodium Polytungstate at a density of 2.4. All samples were rich in dinocysts, except one at 364 cm depth in core CS18 and one at 2026.7 cm in core CS22, which were barren. All percentages are calculated based on the sum of all dinocysts, except varia (indeterminate, indeterminable and reworked specimens) and foraminiferal organic linings. Reworked specimens are identified by their dark colour, reduced relief and stronger opacity. Concentration of palynomorphs is calculated in ml of wet sediment. The P/D ratio is the ratio of the concentration of pollen on dinocysts. It reflects the continentality of the sample (McCarthy and Mudie, 1998). The H/A ratio is the ratio of heterotrophic (dependent on nutrients synthesised by other organisms) taxa on autotrophic (whose energy source is the light) ones. Zonation (on 23 and 22 dinocyst taxa respectively in cores CS22 and CS18) was made by CONISS after square-root transformation, available in the psimpoll software (Bennett, 2007), which was also used for plotting dinocyst diagrams. The diversity was calculated using the Margalef's species richness (Margalef, 1958) and an ordination analysis with non-Metric Multidimensional Scaling (NMDS) (Primer 7; Clarke and Gorley, 2015) allowing distinguishing groups of samples of similar composition.

Identifications were made with the support of the atlas of Mudie et al. (2017), and plates in Marret et al. (2004), Sorrel et al. (2006), Londeix et al. (2009) and Leroy (2010). *Spiniferites cruciformis* specimens were grouped in three different forms (A – standard form, B – pointed apex and C – short and folded processes) as in Marret et al. (2004). *Lingulodinium machaerophorum* ss indicates the sensu stricto form (Leroy et al., 2006; Mertens et al., 2009; Mudie et al., 2017). The "*L.*

machaerophorum bulbous" form has short but clearly bulbous (as in Mudie et al. (2017)) and non-clavate processes. *L. machaerophorum* B is described in Leroy et al. (2006), as having short microgranulate processes with a large striated conical base. *Impagidinium* sp. A is a form defined in Londeix et al. (2009). The name *Spiniferites inaequalis* is conservatively used, although some ongoing discussions propose to move the species to the genus *Impagidinium* (Mertens et al., 2018). In the cumulative diagram, the marine taxa are on the left and the brackish Pontocaspian ones on the right. In the middle, are the heterotrophic taxa and the various forms of *Lingulodinium machaerophorum*. Warm-loving dinocysts are defined by the presence of *Operculodinium israelianum, Spiniferites pachydermus, Polysphaeridinium zoharyi, Tuberculodinium vancampoae* and *Spiniferites mirabilis* as they reflect temperatures higher than nowadays (Marret and Zonneveld, 2003; Londeix et al., 2009; Shumilovskikh et al., 2013; de Vernal et al., 2020; Marret et al., 2020). Seasonal contrast in sea-surface temperature (SST) is reflected by *Bitectatodinium tepikiense, Pentapharsodinium dalei* and *Scrippsiella trifida* (Head et al., 2006; Mudie et al., 2017).

Although not dinocysts, coiled organic linings of foraminifera were found and added to this investigation, rather than to the pollen diagram (Leroy et al., 2023), as they usually belong to the marine environments. The inner organic lining is often produced by benthic foraminifera (de Vernal, 2009; Mudie et al., 2021).

4.2 Other proxies in core CS22

C37 Alkenones were measured in 26 sediment samples from core CS22 between 2050 and 1370 cm. After freeze-drying and grinding, samples were extracted using an accelerated solvent extraction system (ASE350, Thermo Scientific). After a clean-up procedure using silica gel column chromatography with a

mixture of dichloromethane: hexane (1:1), the total lipid extract was analysed by gas chromatography and flame ionization detection (GC-FID, Trace GC, Thermo Scientific). Identification and purity of alkenones were checked in several samples by gas chromatography coupled to quadrupole mass spectrometry (Trace GC DSQII, Thermo Scientific). GC conditions were similar to those described by Sonzogni et al. (1997). Long-chain alkenones are mainly synthesized by marine haptophyte algae (Marlowe et al., 1984) and can been used as an indicator of marine environment in the Sea of Marmara. In the last glacial cycle, no alkenones were detected in sediments of the Sea of Marmara before its connection with the Mediterranean Sea (Vidal et al., 2010).

Benthic foraminiferal faunas were quantitatively investigated in the 125 µm fraction from nine samples. At first a qualitative downcore check of foraminiferal content was performed in the coarse fraction at a 1 m sampling resolution, then refined to 20 cm between 2035 and 1915 cm where very rich benthic foraminifera assemblages were found. Two additional samples were investigated at 1632 and 1631 cm. When possible, 300 specimens were counted in sediment aliquots, and identified to the lowest taxonomic level possible, mainly at the species level. To describe major faunal trends, the species Benthic Foraminiferal Number (BFN, expressed as individuals per g or $ind.g^{-1}$) and frequency data of main species (>1%) were used.

Sediment samples for **diatom and chrysophyte** analyses were collected at 20 cm intervals in each section of core CS22. Smear slides were prepared with a suspension made of known amounts of dry sediment and distilled water. 200 µl of this suspension were spread onto a cover slip, air-dried and mounted on a glass slide using Naphrax mounting medium. Diatom valves were counted along transects

and expressed as number of valves per gram of dry sediment. Chrysophycean cysts were also counted; but morphotypes were not identified.

5 Results

Two main types of dinocyst assemblages were observed (Fig. 3 and 4). The first one is largely dominated by *Spiniferites cruciformis* and *Pyxidinopsis psilata*. By comparison to Black, Marmara and Caspian seas Lateglacial-early Holocene assemblages, they are attributed to brackish Pontocaspian conditions, perhaps in the range of ~7-12 psu, thus clearly lower than the surface conditions of the SoM (Bradley et al., 2012; Marret et al., 2004, 2009, 2019). The second assemblage, called here marine, is an assemblage with diverse taxa also with no direct equivalent in the present. It represents salinities probably close to the surface waters of the modern-day Marmara (Balkis et al., 2016).

5.1 Dinocysts in core CS22

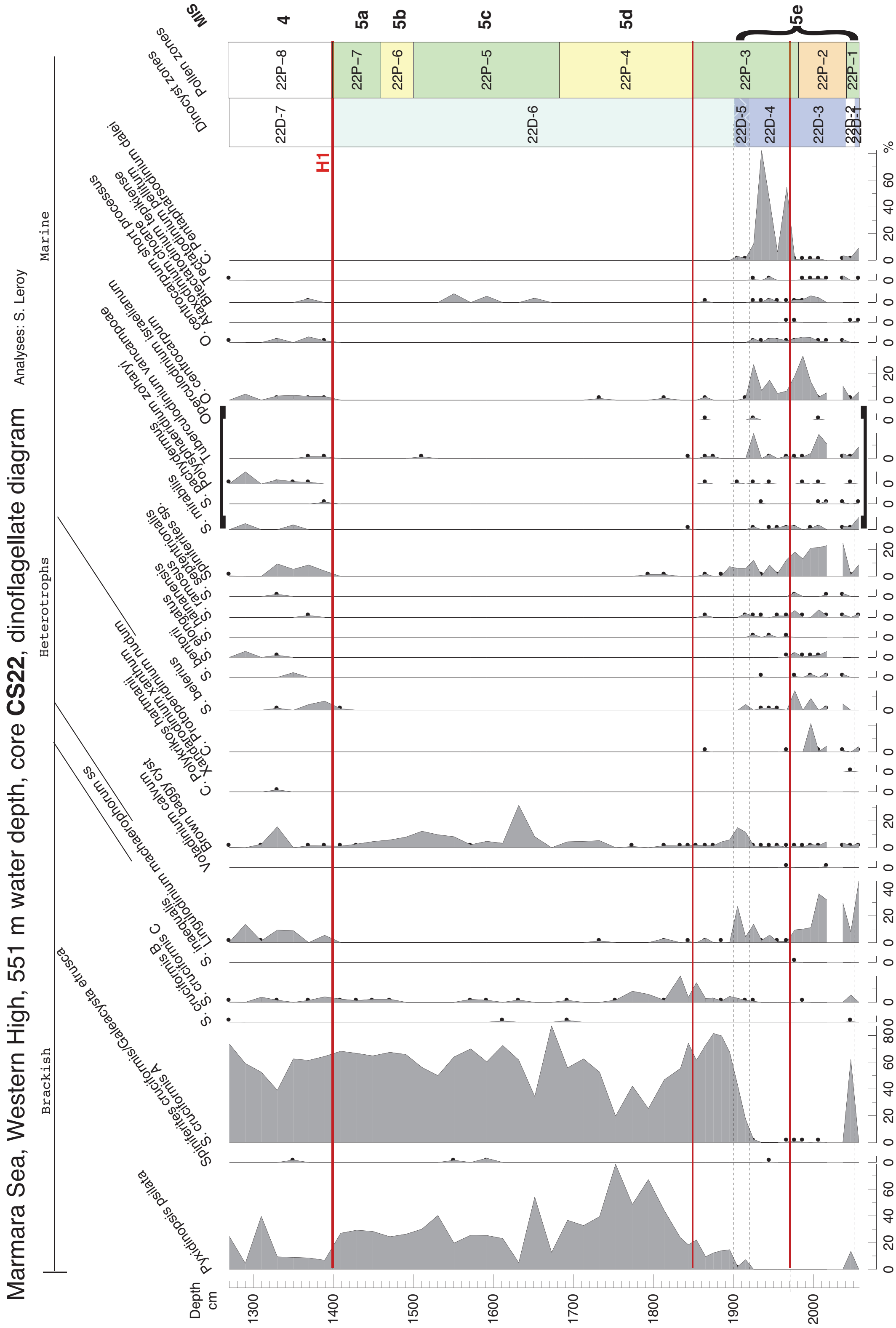
Marmara Sea, Western High, 551 m water depth, core CS22, dinoflagellate diagram
Analyses: S. Leroy
Marine
Heterotrophs
Brackish
MIS
Pollen zones
Dinocyst zones
4
5a
5b
5c
5d
5e
22P-8
22P-7
22P-6
22P-5
22P-4
22P-3
22P-2
22P-1
22D-7
22D-6
22D-5
22D-4
22D-3
22D-2
22D-1
H1
Depth cm
Pyxidinopsis psilata
Spiniferites cruciformis A
Lingulodinium machaerophorum ss
Brown baggy cyst
Votadinium calvum
S. belerius
S. mirabilis
S. pachydermus
Operculodinium centrocarpum
Ataxiodinium choane
Bitectatodinium tepikiense
Tectatodinium pellitum
%

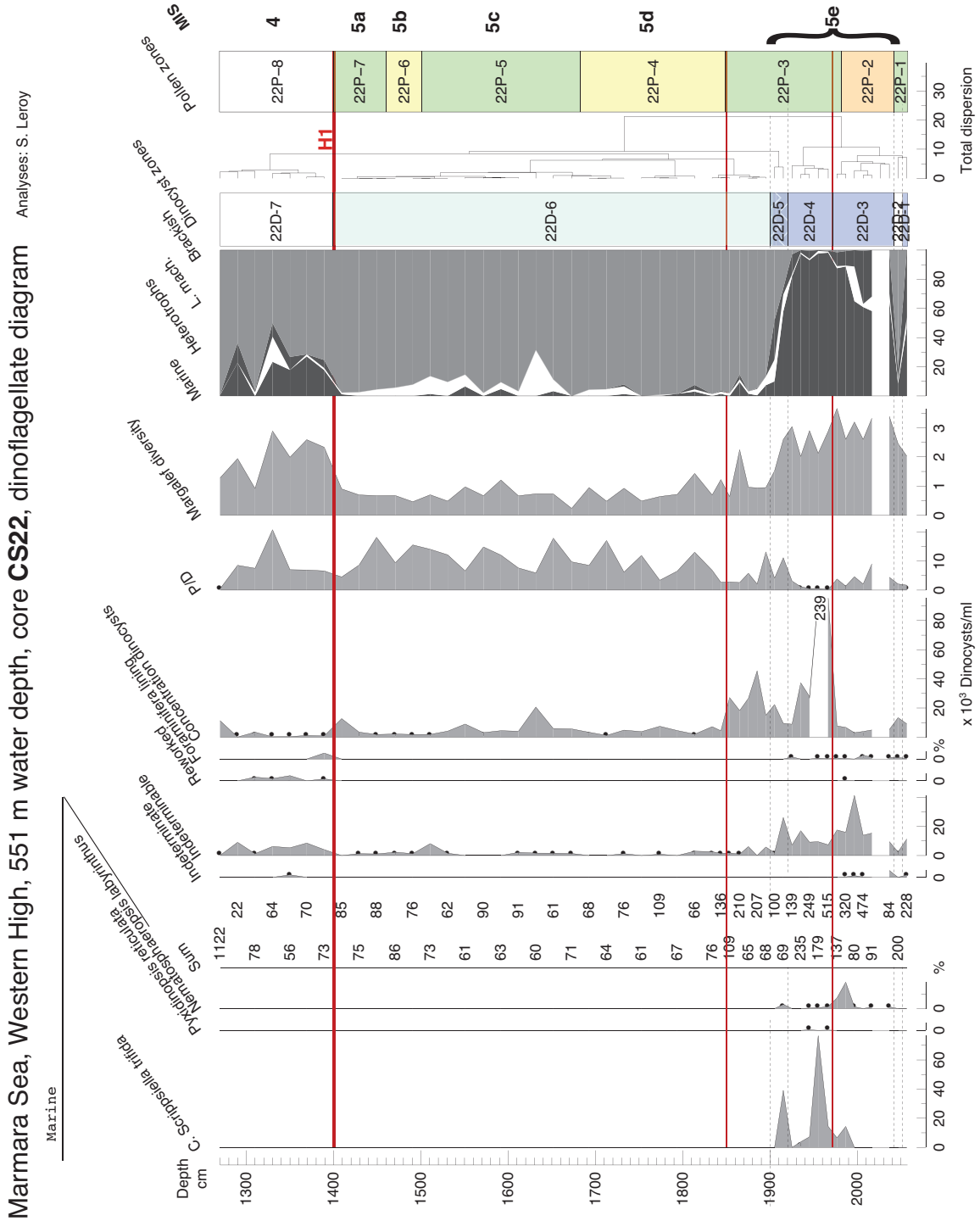

Figure 3 a and b: Percentage dinocyst diagram of core CS22. Black dots for < 5%. Pollen zones to the right with chronological attributions. Horizontal brackets indicate the warm indicators in the marine group. In the cumulative diagram, the marine taxa

are on the left and the brackish Pontocaspian ones on the right. In the middle, are the heterotrophic taxa and the various forms of *Lingulodinium machaerophorum*.

The dinocyst assemblages show a diversity from 3 to 19 taxa, with notably higher numbers of taxa at the bottom of the core, i.e. below 1920 cm (Fig. 3). Broadly, the record shows a succession of two main assemblages, one mostly dominated by marine taxa, and the following one by brackish Pontocaspian taxa. The main change in the diagram according to the CONISS analysis is by far between zones 22D-4 and 5 at 1920 cm depth (Fig. 3). However, it is not sharp.

Zones 22D-1 and D-2 each consist of one sample (at 2057 and 2047 cm depth). In rapid alternation, the first assemblage is marine with a dominance of *L. machaerophorum* alongside: *Spiniferites sp., S. mirabilis*, cysts of *Pentapharsodinium dalei* and *Tuberculodinium vancampoae*. The second sample has a brackish Pontocaspian assemblage, with the dominance of *Spiniferites cruciformis* A and *Pyxidinopsis psilata* and low occurrence of *L. machaerophorum*. Foraminifera linings are observed in zones D-1 to D-4.

Zone 22D-3 (2042-1972 cm depth): Besides zone 22D-1, *L. machaerophorum* displays its highest values here, declining only in the last third of this zone. The percentages of *Operculodinium centrocarpum* increase progressively to a maximum at the end of this zone. *Spiniferites* sp. also has maximal values. The other taxa, mainly marine, are rather diverse (high Margalef diversity index). A high number of indeterminable cysts occur. The sample at 2027 cm depth is rich in pollen, but hardly contains any dinocysts.

Zone 22D-4 (1972-1920 cm depth): The assemblage is still marine and diverse, but rather different from the previous zone. The spectra are alternatively dominated by cysts of *P. dalei* and cysts of *Scrippsiella trifida*. *L. machaerophorum* is present but in small amounts. The P/D ratio is at its minimum, largely because the concentration in dinocyst is very high, i.e. >230,000 cysts/ml. The number of indeterminable cysts is decreasing but still significant.

Zone 22D-5 (1920-1900 cm depth): This zone is a period of transition with the percentages of *S. cruciformis* A progressively increasing, and those of *P. psilata* starting a continuous curve, while the marine forms are less diverse (decreasing Margalef diversity index). *L. machaerophorum* makes a brief return. Brown baggy cysts form a bell-shape curve. *Operculodinium centrocarpum* has nearly disappeared. Cysts of *S. trifida* peak in one of the samples.

Zone 22D-6 (1900-1399 cm depth): This very long (5 m) and rather homogenous (minimal Margalef diversity index) zone is largely dominated by brackish Pontocaspian taxa such as *S. cruciformis* and *P. psilata*. Brown baggy cysts are occasionally more frequent, especially at 1632 cm depth (32%). *Bitectatodinium tepikense* is only sub-continuously present in the middle of this zone between 1652 and 1551 cm depth. *L. machaerophorum* is occasionally present at the beginning of this zone and soon disappears. All through this zone, the P/D ratio is relatively high. Cyst concentration drops drastically at the very beginning of this zone and remains low for the rest of the sequence.

Zone 22D-7 (1399-1270 cm depth): The values of *S. cruciformis* remain the same as in the preceding zone, but those of *P. psilata* significantly drop. The assemblage is diverse with many marine forms but with a low occurrence. *L. machaerophorum* is back with irregular presence between 0.2 and 14 %. Three foraminifera linings (4%) were found at the base of this zone. Concentration is varying, at times below 500 dinocysts/ml. Reworked elements are frequent.

5.2 Dinocysts in core CS18

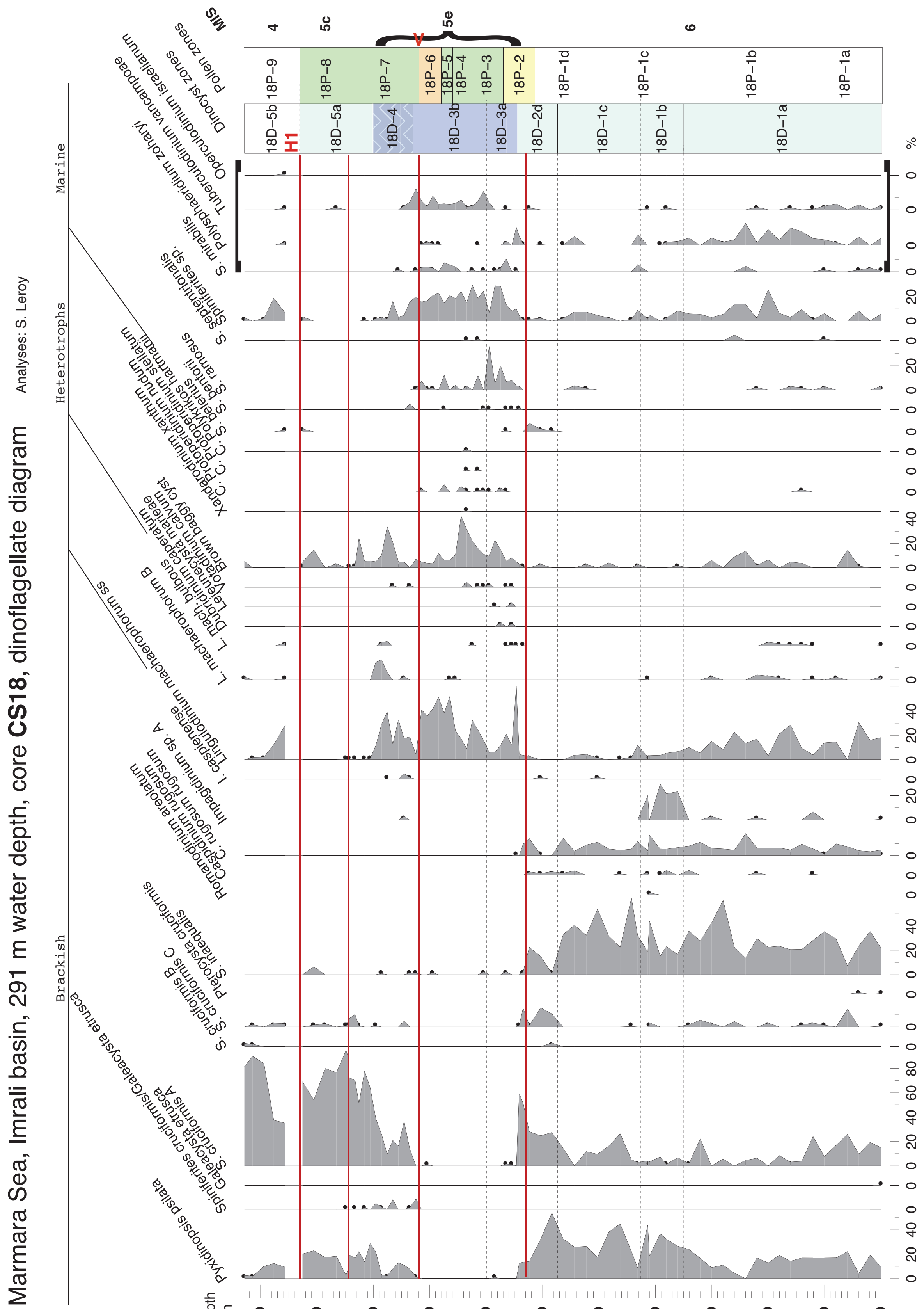

Marmara Sea, Imrali basin, 291 m water depth, core CS18, dinoflagellate diagram
Analyses: S. Leroy
Marine
Heterotrophs
Brackish
MIS
Pollen zones
Dinocyst zones
Operculodinium israelianum
Operculodinium vancampoae
Tuberculodinium zoharyi
Polysphaeridium
S. mirabilis
S. septentrionalis
Spiniferites sp.
S. ramosus
S. bentorii
S. hartmanii
S. belerius
Polykrikos stellatum
C. nudum
Protoperidinium
Xandarodinium xanthum
Brown baggy cyst
Votadinium calvum
Bitectatodinium
L. machaerophorum B
Lingulodinium machaerophorum ss
I. caspienense
Lingulodinium sp. A
Impagidinium rugosum
C. rugosum
Caspidinium
Romanodinium areolatum
Pterocysta cruciformis
S. inaequalis
S. cruciformis B C
S. cruciformis/Galeacysta etrusca
Spiniferites cruciformis/Galeacysta etrusca
Galeacysta etrusca
S. cruciformis A
Pyxidinopsis psilata
Depth cm
H1
18D-5b
18D-5a
18D-4
18D-3b
18D-3a
18D-2d
18D-1c
18D-1b
18D-1a
18P-9
18P-8
18P-7
18P-6
18P-5
18P-4
18P-3
18P-2
18P-1d
18P-1c
18P-1b
18P-1a
4
5c
5e
6
%

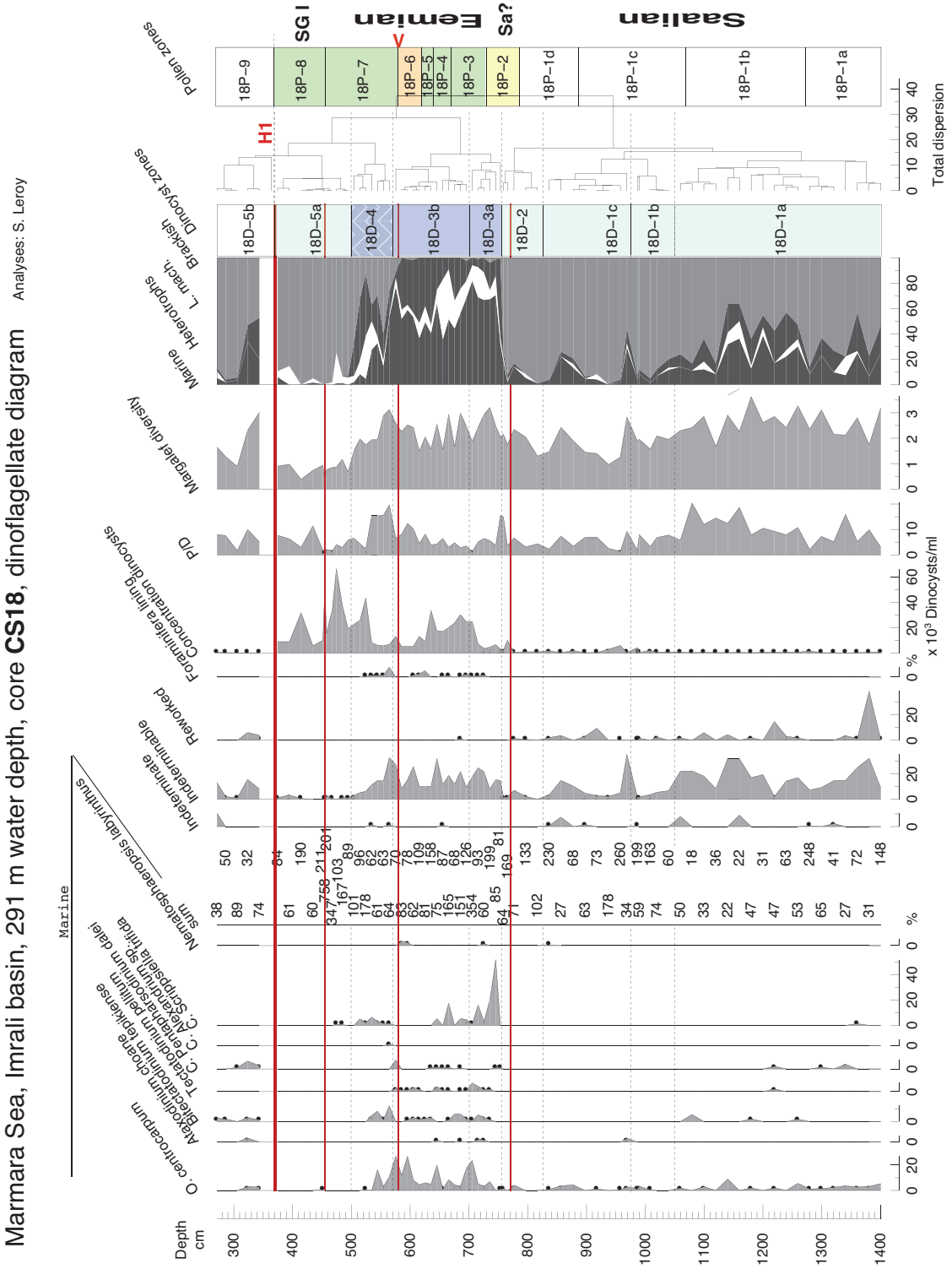

Figure 4 a and b: Percentage dinocyst diagram of core CS18. Black dots for < 5%. Pollen zones to the right with chronological attributions. Horizontal brackets indicate the warm indicators in the marine group. In the cumulative diagram, the marine taxa

are on the left and the brackish Pontocaspian ones on the right. In the middle, are the heterotrophic taxa and the various forms of *Lingulodinium machaerophorum*.

The dinocyst assemblages show a diversity from 3 to 17 taxa, with notably higher numbers of taxa below 1180 cm, and at 735 and 565 cm (Fig. 4). Broadly, the record shows the succession of three main assemblages, one mostly dominated by marine taxa in the middle, with below and above it two brackish Pontocaspian assemblages of two different types. The two main changes in this diagram are at 756 and 570 cm depth (Fig. 4).

Zone 18D-1, 1400.5 – 826.5 cm depth: This is a very long zone of nearly 6 m. It is dominated by brackish Pontocaspian taxa such as *P. psilata*, *S. cruciformis* A, *S. inaequalis* and *Caspidinium rugosum rugosum,* with a significant occurrence of *L. machaerophorum ss*. In general, concentrations are relatively low, mostly below 1000 cysts/ml. Reworked cysts are frequent. This zone has been subdivided into three subzones, with subdivisions as followed. Subzone 18D-1a (1400.5-1049.5 cm) is dominated by *S. inaequalis*. *L. machaerophorum ss, P. psilata* and *S. cruciformis* A are abundant. A range of marine and brackish Pontocaspian taxa occur side by side. Indeterminable dinocysts are abundant. A large peak of reworked cysts occurs at 1381 cm depth. The P/D ratio remains high all through this zone, with maximal values towards the end, i.e. a maximum of up to above 20. Concentrations are very low, often lower than 500 cysts per ml. Subzone 18D-1b (1049.5-977 cm): This zone is characterised by a bell-shaped curve of *Impagidinium* sp. A. *S. inaequalis* is still abundant. *P. psilata* displays increasing values across this zone. In subzone 18D-1c

(977-826.5 cm)*, P. psilata* reaches maximal values, i.e. 54%. The percentages of *S. inaequalis* are still high. Less diverse marine forms are observed.

Zone 18D-2, 826.5-756 cm depth: This zone is characterised by many changes. *P. psilata* decreases and *S. cruciformis* A increases up to a brief maximum of 59%. *S. cruciformis* C is very abundant. A small bell-shaped curve of *S. belerius* occurs. *S. inaequalis* values drop. Very few marine taxa subsist. Concentrations are slightly increasing. Before the end of this zone a hiatus occurs at 772 cm. Finally, the limit 18D-2 and 18D-3 at 756 cm is recognised as one of the strongest statistical changes according to CONISS.

Zone 18D-3, 756-570 cm depth, is a totally different zone, with *L. machaerophorum* (up to 52%) and *Spiniferites* sp. (up to 30%) widely dominant. Brown baggy cysts are very abundant in this zone and the following one, i.e. up to 30%. Many marine taxa are present. *S. ramosus*, *O. centrocarpum* and *Tuberculodinium vancampoae* are well represented. Concentrations are high, often around 10,000-20,000 dinocysts/ml. A split into subzones 3a and 3b at 700.5 cm depth is based on a maximum of *S. ramosus,* very large peak of cysts of *S. trifida* (52%), medium-high concentration and maximum percentage of marine taxa in subzone 3a; whilst in subzone 3b high *T. vancampoae* and high concentration occur. This zone ends with the second strongest diagram change (as calculated by CONISS). Foraminiferal linings are only present in this zone and in the following zone.

Zone 18D-4, 570–499.5 cm depth, appears as a transition, with mixed marine and brackish Pontocaspian assemblages. *P. psilata* and *S. cruciformis,* quasi absent in

zone 18D-3, reappear. *L. machaerophorum* (with a peak of other forms of *L. machaerophorum* towards the end of this zone) and brown baggy cysts are still abundant. Marine taxa remain present, but their values decrease. Concentrations, after moderate values, become high again. P/D is maximal, i.e. up to just below 20.

Zone 18D-5, 499.5-271.5 cm, is split in two by the seismic red-H1 reflector; moreover, a barren sample occurs a few cm above this stratigraphic hiatus. In subzone 18D-5a, 499.5-369 cm depth, *S. cruciformis* A very largely dominates with percentages up to 95%. Besides *P. psilata* and brown baggy cysts, hardly any other taxa are present. It is noteworthy that *L. machaerophorum* has only rare occurrences in this subzone, and only at its base. This is a very low diversity subzone (minimum in the Margalef index). Concentrations, after being very high, become high, i.e. 66,000 to 10,000 dinocysts/ml. Subzone 18D-5b, 369-271.5 cm depth: The assemblages are similar to subzone 18D-5a (dominance of brackish Pontocaspian taxa), but brown baggy cysts have quasi disappeared and are replaced by *L. machaerophorum* that have re-appeared. A moderate range of marine taxa is present. Concentrations are very low as in subzones 18D-1a. Reworked elements are common in the lower half of this subzone, just above the barren sample.

5.3 Other proxies in core CS22

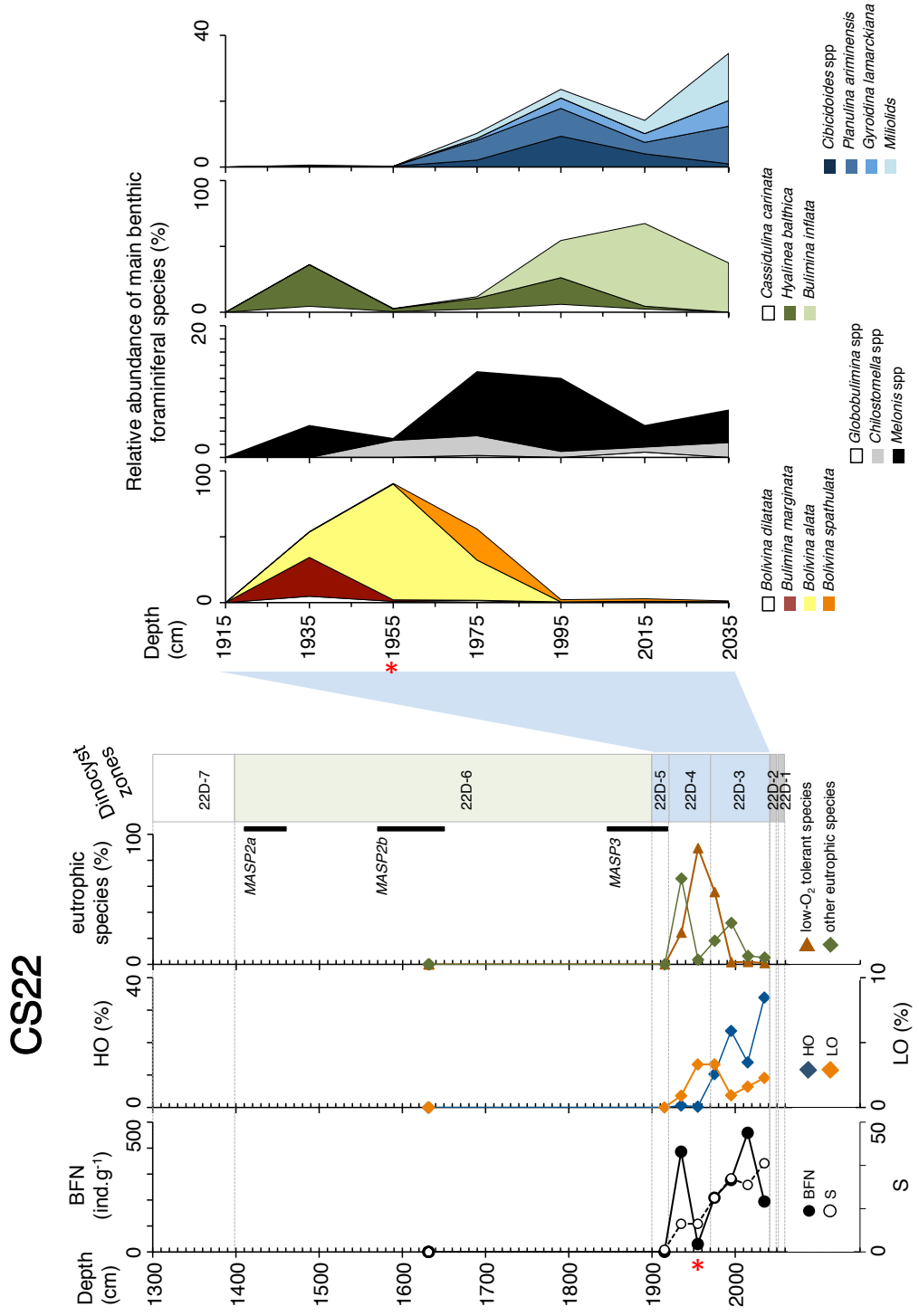

Figure 5: Benthic foraminiferal record of core CS22 with dinozones and Marmara sapropels (MSAP). Right panel: relative abundance of main species (>3%) between 2035 and 1915 cm depth. Left panel: Benthic Foraminiferal Number, BFN (ind.g^{-1}),

468 species richness S, relative abundance of ecological groups of species. HO =
469 species adapted to high-oxygen level, LO = low-oxygen indicators, eutrophic species
470 = species adapted to high organic carbon fluxes. For further explanation on
471 ecological assignment of species, the reader is referred to the discussion and Table
472 SI2.
473
474 Quantitative investigation of benthic foraminiferal assemblages relies on the
475 recovery of a well-preserved, abundant (164 to 361 specimens) and diverse (>60
476 species overall) faunal content between 2035 and 1915 cm depth (Table SI1). Apart
477 from a few individuals (< 10) belonging to neritic taxa (e.g. *Ammonia*, *Discorbinella*,
478 *Elphidium*), assumed to be post-depositional, foraminiferal assemblages
479 overwhelmingly consist of species from marginal to bathyal environments. The BFN
480 ranges from 30 to 459 ind.g^{-1}, with lowest values recorded at 1955 cm. Dominant
481 species (>5%) belong to *Bolivina* spp, *Bulimina* spp, *Cassidulina carinata*,
482 *Cibicidoides* spp, *Hyalinea balthica* and *Melonis* spp and indicate fully marine
483 conditions at the seafloor at the base of the core. The foraminiferal record, though
484 short, exhibits a marked species shift between 1995 and 1975 cm (Fig. 5). From
485 2035 to 1995 cm, species number is highest, ranging from 31 to 41. Faunas are
486 strongly dominated by *Bulimina inflata* (28-63%), together with various associated
487 species including *Cibicidoides* spp (1-9%), *Gyroidina lamarckiana* (3-8%), *Planulina*
488 *ariminensis* (3-11%) and miliolids (3-14%). Minor species (<3%) include *Bulimina*
489 *aculeata*, *Uvigerina mediterranea* and *U. peregrina*. From 1975 up to 1935 cm, most
490 of the afore-mentioned species disappear from the record. Dominant species consist
491 mainly in *Bolivina alata*, *B. spathulata* and *Bulimina marginata*, which collectively
492 account for 49 to 90% of the assemblage. Concomitant to this faunal shift, species

number drops from 25 to 13 (Fig. 5). By contrast, several other species such as *Cassidulina carinata*, *Hyalinea balthica*, *Melonis affinis* and *M. pompiloides* exhibit no clear upcore trend. Present along the whole record, these species show punctual increases, as especially marked for *H. balthica* at 1995 (32%) and 1935 (20%) cm. Sample at 1915 cm is considered barren of benthic foraminifera as fourteen reworked individuals only were found. Samples at 1632 and 1630 cm were devoid of any foraminifera.

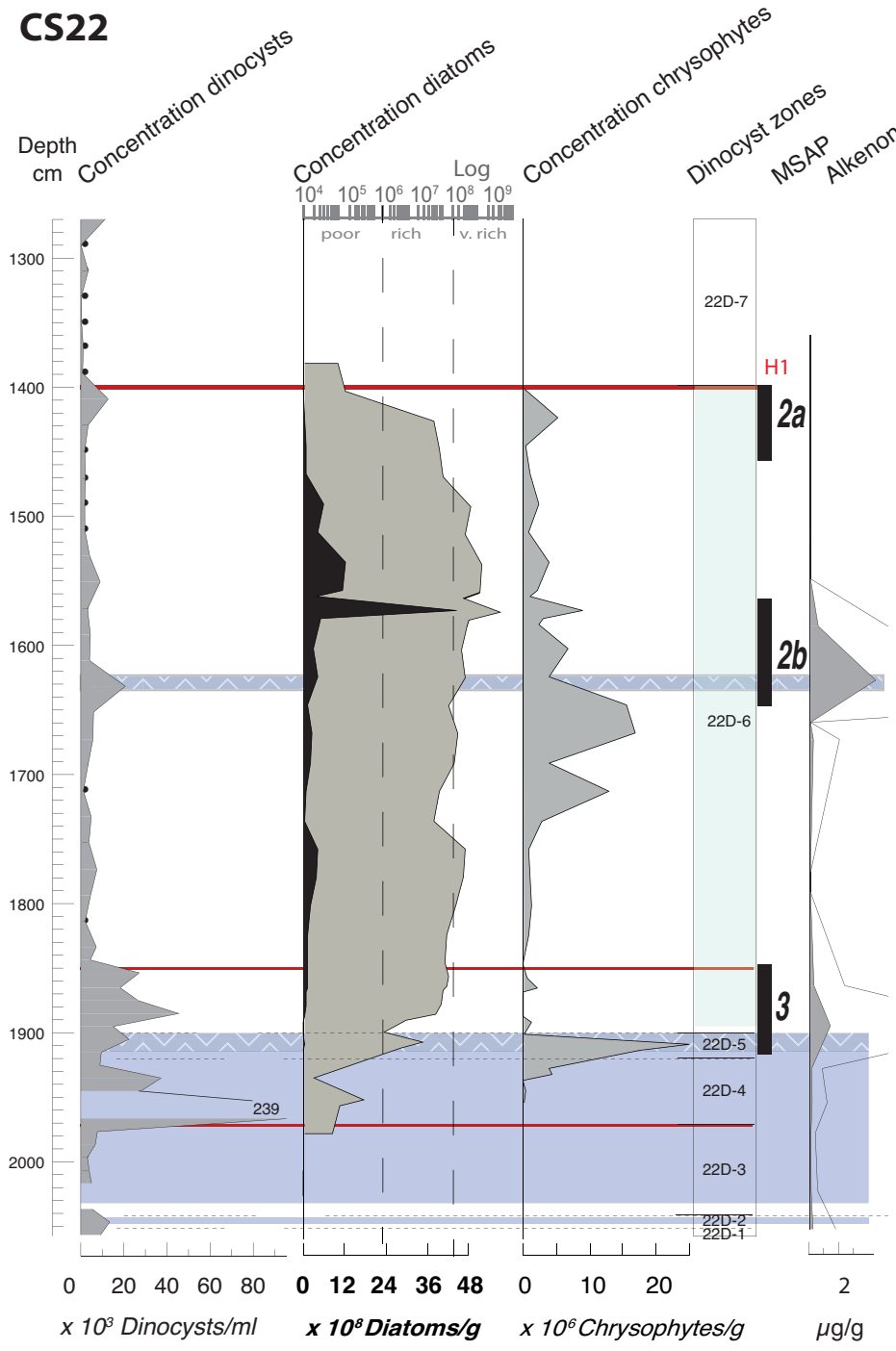

500

501 **Figure 6:** Palaeoproductivity: concentrations of dinocysts, diatoms (in decimal and
502 log scales) and chrysophytes, with dinozones, C37 alkenones (thin black line curve
503 for 10 x exaggeration) and Marmara sapropels (MSAP) in core CS22. The
504 concentration of C37 alkenones in µg/g are based on dry weight sediment. The
505 second marine phase at 1633-1632 cm depth is indicated by a box with a blue
506 zigzag highlight.

Diatom preservation is becoming better from bottom to the red-H1 reflector. Hardly any diatoms were found below 1915 cm (Fig. 6). Then only some occurrences are noted between 1915 and 1866 cm. From 1854 cm upwards and until 1470 m, the diatom concentrations are high to very high. Diatom concentrations are highest between 1591 and 1491 cm depth. Chrysophycean cysts are abundant when diatom concentrations decrease. The diatom assemblages are composed of a mixture of fresh and brackish-water species. Dominant *Stephanodiscus* species (*S. minutulus, S. parvus, S. medius, S. neoastrea, S. hantzschii*) occurred with numerous fragments of *Entomoneis calixasini*, a fossil species so far only found in core sediments of the SoM (Pailles et al., 2014). The first occurrence of *E. calixasini* in core CS22 is recorded at 1834 cm depth. Spores of a marine planktonic diatom, *Chaetoceros,* are observed from 1850 to 1830 cm.

The values of alkenones are usually below detection limit, except at 2050-1865 cm and 1633-1592 cm, reaching respective maxima of 1.3 µg/g at 1896 cm and 4.4 µg/g at 1633 cm depth (Fig. 6).

6 Interpretation and discussion

6.1 Core CS22: taphonomy, surface water condition and chronology

6.1.1 Taphonomy

Below the sapropel

At 2027 cm in zone 22D-3, the sample is unexpectedly barren in dinocysts. It is one of the samples of zone 22P-2 with abundant *Pinus* pollen (76%) (Leroy et al., 2023). The lithology shows a bioturbated sediment. Sediment disturbance may also

contribute to explain the rapidly changing spectra in the short zones 22-D1 and D2. The sharp zone limit at 1920 cm (between zones 22D-4 and 5) corresponds to a very thin silt layer and a change from bioturbated to unbioturbated sediment, that is the start of the sapropel attributed to MSAP-3 (1920-1853 cm).

In the sapropel and until the red-H1 seismic reflector

Dinocysts (as well as pollen) are well preserved. Their concentrations are high in all sapropels as observed in other sapropels (Cheddadi and Rossignol, 1995; Kotthoff et al., 2008) (Fig. 6).

Impact of red-H1 seismic reflector

The red-H1 reflector corresponds to a widespread erosion event in the Sea of Marmara that causes hiatuses of spatially variable duration across the transition from MIS 5 to 4 (Grall et al., 2014; Çağatay et al., 2019). The sediment deposited after the hiatus is dated as MIS 4 based on magnetic paleo-intensities (in core CS 22; Kende, 2018) and on tephra correlations (in cores CS18 and CS 27; Wulf et al., 2021). With the red-H1 reflector, a long-term change in taphonomy is initiated in the SoM. It is seen in the reworking of older marine layers and of soils. Firstly, some foraminifera (organic linings) are brought in the sediment. Secondly, the non-pollen palynomorphs *Glomus* (a fungal spore) is present, due to inwash of soil erosion products (Leroy et al., 2023). This reflects a turning point in the aquatic conditions of the SoM.

552 *6.1.2 Sea-surface and bottom conditions*

553 The depths of 2042-1920 cm (dinocyst zones 22D-3 and 4) are fully marine.
554 This is clearly seen not only in the dinocyst assemblages, but also in the presence of
555 alkenone and in the benthic foraminiferal content (Fig. 3, 5 and 7).

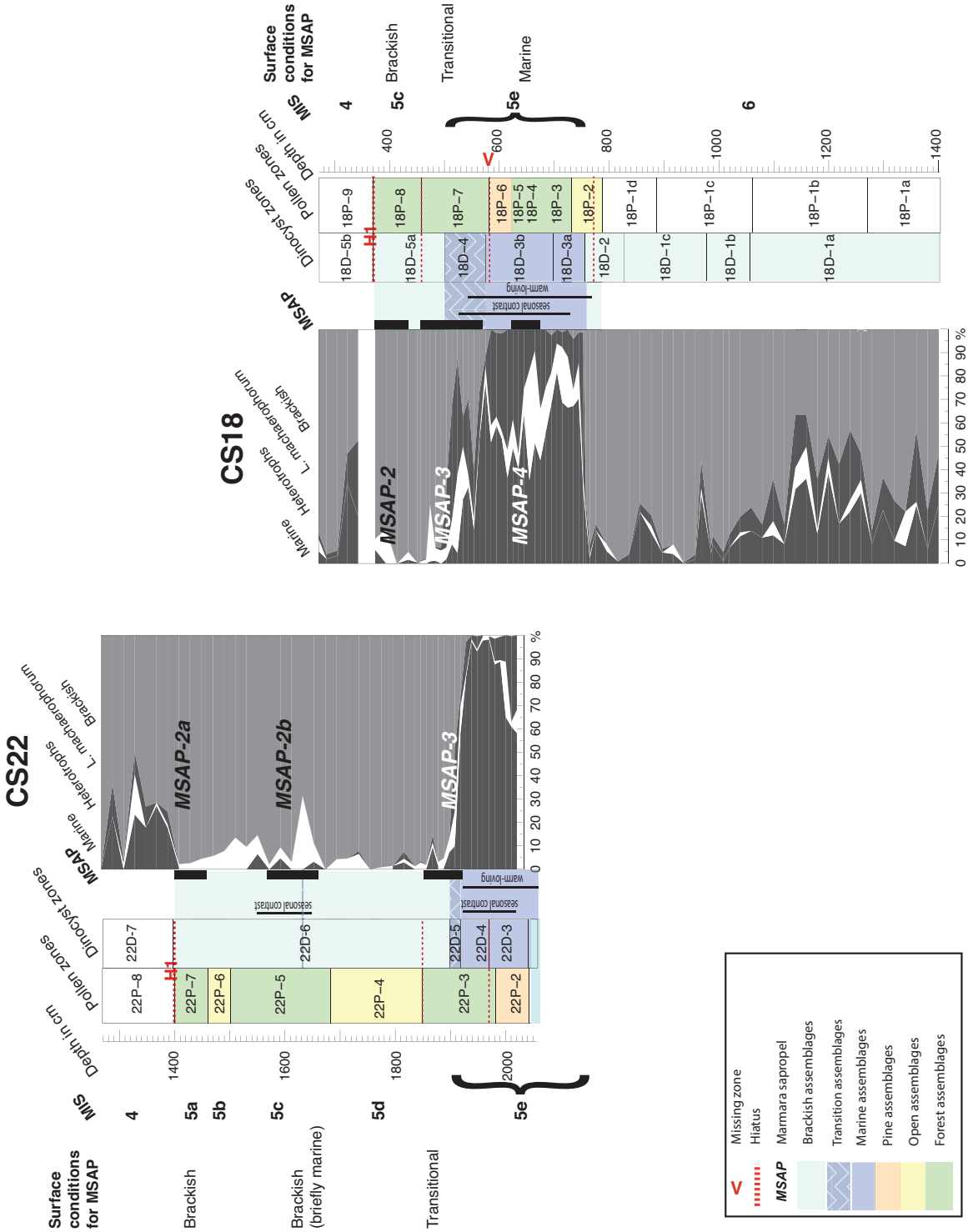

556

Figure 7: The cumulative diagrams sorting dinocyst groups/taxa by salinity. The four groups are the marine ones (black) to the left, the brackish Pontocaspian dinocysts (grey) to the right), and in the middle the heterotrophic cysts (white) and the *Lingulodinium machaerophorum* forms (black). Dinocyst zones: blue highlight for marine, light blue for brackish Pontocaspian. The distribution of warm-loving and seasonal contrast indicators as vertical black lines. Pollen zones: green highlight for high arboreal taxa (minus *Pinus*) zones and yellow for low arboreal taxa % and high *Pinus* % zones.

Five indicators of warm sea-surface temperature (SST) are recorded: *O. israelianum, S. pachydermus, P. zoharyi, T. vancampoae* and *S. mirabilis* (Fig. 3 and 7). They are especially abundant in zone 22-D3. Their occurrence suggests temperatures higher than nowadays. *B. tepikiense,* occurring in zones 22-D3 and 4, reflects marine conditions with seasonal amplitudes of SST. Thus, conditions recorded in zone 22-D3 suggest a warm climate with seasonal contrast.

In zone 22D-4 at 1955 cm, high values of cysts of *P. dalei* and *S. trifida* suggest an increase in temperature seasonality and lower salinity (e.g. Head et al., 2006; Mudie et al., 2017). In contrast, very high concentrations point at surface waters rich in nutrients and possibly bottom waters with low oxygen (Mudie et al., 2017). This may be due to alternating deep-water upwelling - when the heavy saline marine waters penetrate the bottom of the basin from the Aegean Sea - and stratification. This occurs below the horizon with high TOC (sapropel MSAP-3 at 1920-1853 cm depth and bottom anoxia, Fig. 2).

To tackle environmental changes at the seafloor, the approach of Cornuault et al. (2016, and references therein) was followed and foraminiferal species were

582 gathered into three functional groups assumed to be representative of contrasted
583 oxygen and trophic conditions at the seafloor: (1) species adapted to high oxygen
584 conditions (HO), (2) low-oxygen indicators (LO), and (3) species adapted to
585 eutrophic conditions (Fig. 5). Ecological assignment is given in Table SI2. The major
586 faunal shift observed at 1995 -1955 cm suggests contrasted oxygen conditions
587 between zones 22D-3 and 22D-4, possibly related to the establishment of eutrophic
588 conditions. In zone 22D-3, benthic foraminiferal assemblages are ecologically
589 diverse and consist of a mix of epibenthic and various endobenthic species. This
590 sequence and the high abundance of HO species suggest a mesotrophic
591 environment where well-oxygenated conditions prevailed at the seafloor. By contrast,
592 HO indicators disappearance in zone 22D-4 together with high abundance of species
593 adapted to high organic fluxes points to reduced oxygen level during this phase.
594 Assemblages from this zone are successively dominated by species adapted to
595 contrasted oxygen conditions, suggesting variable oxygenation level during zone
596 22D-4. In particular, the BFN decrease, high dominance of eutrophic species tolerant
597 to low-oxygenation and slight increase of LO species suggest dysoxic conditions at
598 the beginning of this period at 1935 cm, high dominance of species adapted to
599 moderate oxygen depletion strongly suggest environmental changes recorded at the
600 seafloor directly are related to eutrophication rather than ventilation changes.
601 Overall, foraminiferal faunas preceding MSAP-3 deposition exhibit strong similarity
602 with assemblages reported in organic-rich layers from Holocene and Late Glacial
603 archives in the SoM, similarly dominated by various Bolivids and Buliminids, among
604 other species (e.g. Çağatay et al., 2000; Kaminski et al., 2002; Kirci-Elmas, 2008).
605 Our benthic record thus matches well the establishment of water column stratification

606 and bottom water hypoxia prior to sapropelic deposition, and indicates anoxic
607 conditions do not prevail at the seafloor in zones 22D-3 and 22D-4.
608 In the dinocyst diagram (Fig. 3), the P/D ratio, informing on the intensity of
609 terrestrial influence on the aquatic realm, is extremely low in zone 22-D4. It is low in
610 general below the hiatus at 1845-1842 cm depth. It is relatively high above it with
611 values frequently higher than 10. It is therefore suggested that the water level was
612 the highest in zone 22-D4 (1972-1920 cm). This is just before the high TOC values
613 linked to the MSAP-3 sapropel.
614
615

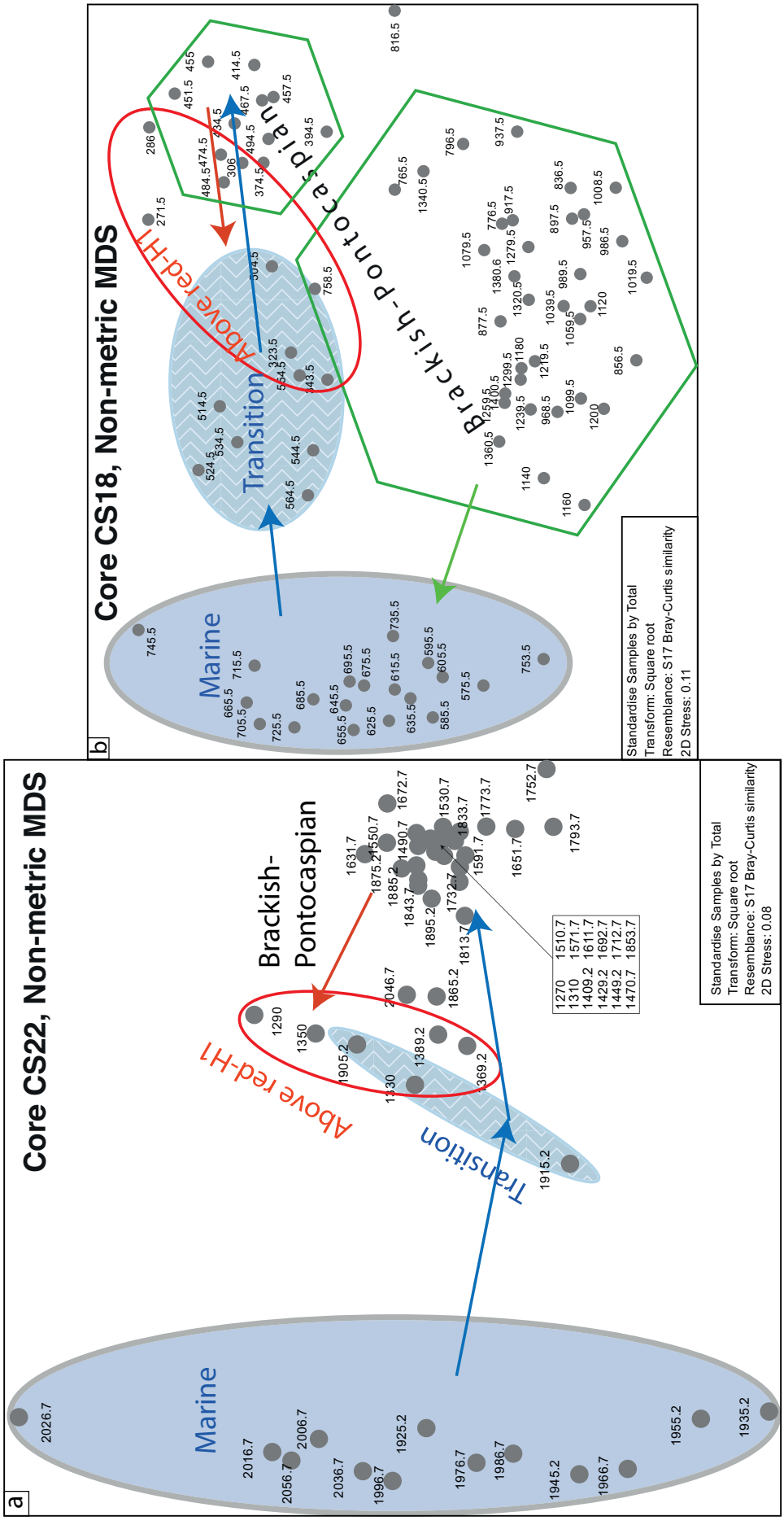
a
Core CS22, Non-metric MDS
Marine
Transition
Above red-H1
Brackish-Pontocaspian
Standardise Samples by Total
Transform: Square root
Resemblance: S17 Bray-Curtis similarity
2D Stress: 0.08
b
Core CS18, Non-metric MDS
Marine
Transition
Above red-H1
Brackish-Pontocaspian
Standardise Samples by Total
Transform: Square root
Resemblance: S17 Bray-Curtis similarity
2D Stress: 0.11

616

Figure 8: Results of the NMDS analysis on dinocyst percentages from cores CS22 (a) and CS18 (b). Depth in cm.

Zone 22D-5 (1920-1900 cm) is a transition zone towards brackish Pontocaspian conditions (also seen in the NMDS results in figure 8). The disappearance of foraminiferal shells at 1915 cm is attributed to bottom anoxic conditions in the subsequent MSAP-3 (1920-1853 cm).

Then zone 22D-6 (1900-1399 cm) is clearly brackish Pontocaspian, as seen in dinocysts and in the diatom species that indicate fresh to brackish conditions. Interestingly, marine *Chaetoceros* spores occur at 1850-1830 cm. The highest concentrations of Chrysophycean cysts indicating fresher / more oligotrophic conditions occurred between 1680 and 1611 cm depth when diatom concentration decreases. Later, between 1591 and 1491 cm, the highest diatom concentrations recorded suggest increased seasonal productivity.

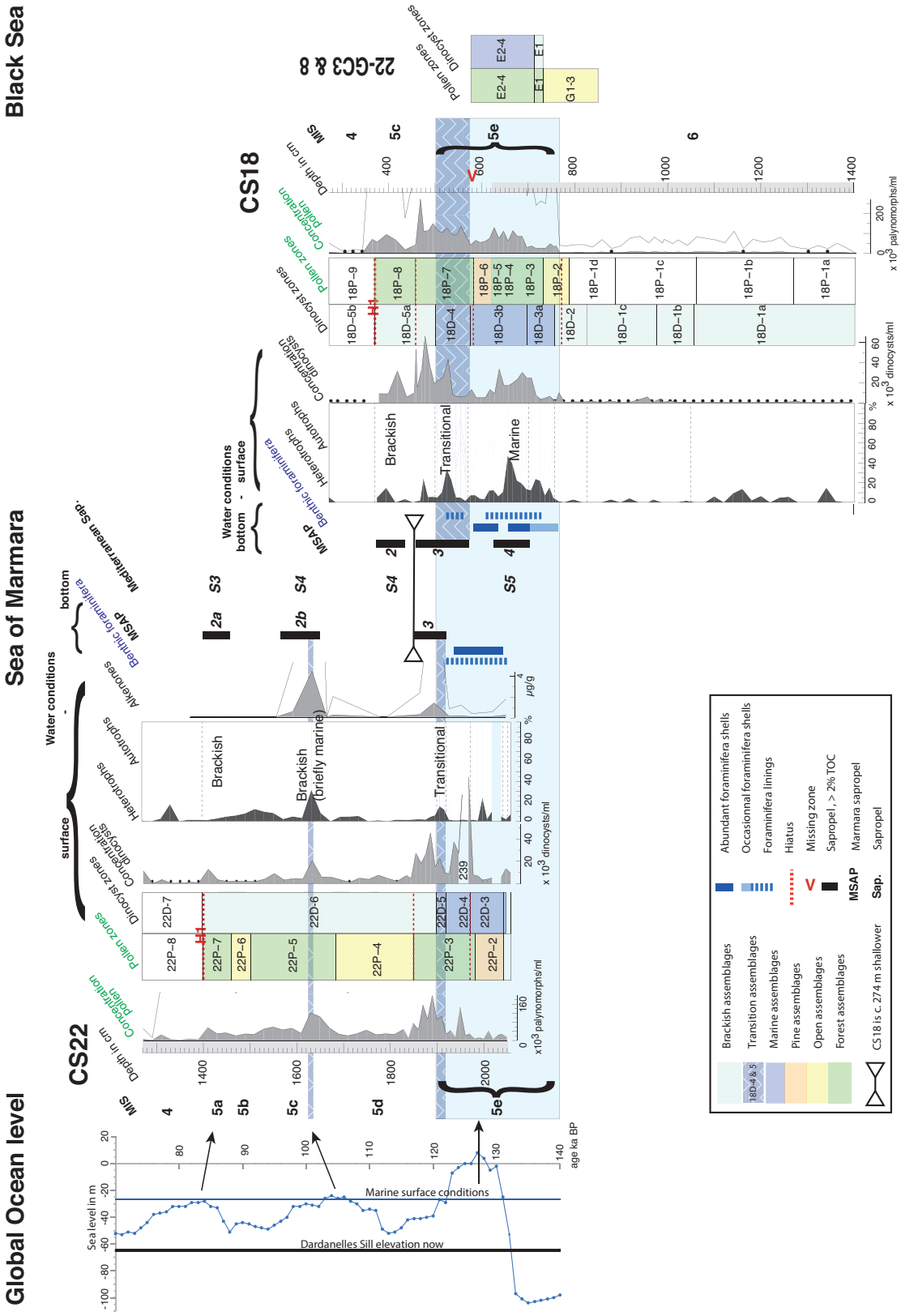

631

632 **Figure 9**: Water conditions. At the surface, dinocyst concentration and the

633 ratio heterotrophic and autotrophic dinocysts (H/A). In the middle for core CS22, also

634 the alkenones. For the bottom: Marmara sapropels (MSAP, >2% TOC), benthic

foraminifera shells and benthic foraminifera organic lining. The top of the marine horizon in core CS18 (hiatus between zones 18P-7 and 8) is c. 274 m deeper than that in core CS22 (hiatus between zones 22P-3 and 4). Horizontal bold V for pollen and dinocyst zones absent in core CS18. For linking with the sister paper on pollen (Leroy et al., 2023), pollen zones and pollen concentrations are also shown. By combining the two light grey vertical boxes, the most complete record is obtained. Sea-level curve from Rohling et al. (2021) with the position of the Dardanelles Sill elevation now (-65 m) and the sea-level threshold where transition from brackish to marine conditions occurred. The pollen and dinocyst records of the Black Sea cores 22-GC3 & 8 are shown in a simplified way. The records of these cores and of core CS18 are aligned in two ways. First the beginnings of the interglacial (transition yellow to green box infills) should be synchronous and secondly the Black Sea dinocyst sequence should stop before the return of brackish-Pontocaspian dinocysts in Marmara core CS18.However this long 22D-6 zone is not homogenous. At 1632 cm, a peak of heterotrophic dinocyst is observed. It seems to correspond to the second peak in alkenones, indicating marine influence, at 1633 cm (Fig. 9). According to pollen analysis, it is in an interstadial (Saint-Germain I). Thus, a brief marine incursion is probable. It is located at the beginning of sapropel MSAP-2b at 1653-1570 cm.

Zone 22D-7 (above 1399 cm, above the red-H1 seismic reflector) suffers from taphonomical problems (Leroy et al., 2023). Nevertheless, it is mainly brackish-Pontocaspian, but the occurrence of marine taxa can be either attributed to limited marine influences or more likely to reworking (see above).

658 *6.1.3 Elements of chronology*

659 It is suggested that the high sea level of MIS 5e (Bard et al., 1996; Koeling et
660 al., 2009) is represented here by zones 22-D3 to 5. In the whole of MIS 5, it is mainly
661 in the maximum sea level of MIS 5e that the Black Sea would have been connected
662 to the Global Ocean. At that time, the two Marmara straits would have the two-way
663 exchange of water as today. It was established earlier that stratigraphic succession
664 immediately above the red-H1 reflector belongs to MIS 4 (Grall et al., 2014; Kende,
665 2018; Çağatay et al., 2019), which can now be shown to reflect a brackish-
666 Pontocaspian environment. During MIS 4, the SoM was an oligotrophic lake, with no
667 evidence of water body stratification, and was almost certainly disconnected. During
668 the late phases of MIS 5, the inflow of Mediterranean water was restricted and this
669 probably required a Dardanelles Sill depth higher that the present sill depth. We will
670 come back to this point later in the discussion and here only consider the phasing of
671 the marine to brackish transition. In the age model proposed in Çağatay et al. (2019),
672 this transition occurs after MIS 5d (in the 110 to 100 ka interval) at a time of sea-level
673 rise, and that may be considered unlikely. This transition more probably occurred
674 concurrently with sea-level drop either later in MIS 5c or during the transition from
675 MIS 5e to 5d. Assigning this transition to later in MIS 5c would keep the sapropel
676 correlation proposed by Çağatay et al. (2019) but imply that MIS 5d is not observed
677 in the pollen record in either core (Leroy et al., 2023).

678 ## 6.2 Core CS18: taphonomy, surface water condition and chronology

679 *6.2.1 Taphonomy*

680 Before the transition 18D-2 to 3 (756 cm) towards marine assemblages, thus
681 already at the beginning of pollen zone 18P-2 (786.5-730.5 cm), one may see

682 sudden changes. This is firstly a sediment change from homogenous to finely
683 laminated around 772 cm. Two round pebbles (of river origin?) are found at 775 and
684 758.5 cm. In between them, one finds a 2 mm-thick silt layer (773 cm). Moreover, at
685 771 cm a sharp increase of the concentration in pollen and spores (from <5000 to >
686 25,000 palynomorphs/ml) and at 762 cm a sharp and long-lasting reduction of the
687 reworked pollen. The sharp statistical limit at 756 cm in the dinocyst diagram is 17
688 cm above the 2 mm-thick silt layer. These observations are in support of an increase
689 of water level with the influx of marine water from the Aegean Sea (Çağatay et al.,
690 2009) leading to sediment disturbance and taphonomical changes.

691 The sharp dinocyst limit at 570 cm is slightly above the hiatus at 580 cm (one
692 sample). It is interesting to note here the absence of the equivalent to zone 22D-4
693 with its very high percentages of cysts of *P. dalei* and *S. trifida*. The sediment in core
694 CS 18 was probably lost by erosion linked to this hiatus.

695 In general, dinocysts and pollen are well preserved in the three sapropels and
696 their concentrations are maximal, as observed in core CS22. Minimal concentrations
697 are reached in MIS6 and 4.

698 After the red-H1 hiatus, a barren sample (neither pollen, nor dinocysts, but
699 many *Dreissena* shell debris) is noted. In the following sample, a peak of *L.*
700 *machaerophorum*, a large peak of reworked pollen, significant presence of reworked
701 dinocysts and abundance of *Glomus* co-occur. Therefore, no marine invasion can be
702 reconstructed; to the contrary a strong coastal, even soil, input should be
703 recognised. The sediment taphonomy changes completely.

704 *6.2.2 Sea-surface conditions*

705 The transition from brackish Pontocaspian to fully marine conditions (zones
706 18D-2 to 3, main change highlighted by CONISS) seems to occur very abruptly at

707 756 cm depth (Fig. 4 and 7). Then in zone 18D-3, the conditions are only fully
708 marine. Zone 18D-4 is a transitional period, back towards a brackish-Pontocaspian
709 environment. This transition zone is also well marked in the NMDS results (see
710 green arrow in Fig. 8). The surface waters of subzone 18D-5a are clearly brackish-
711 Pontocaspian. Subzone 18D-5b is mostly brackish-Pontocaspian but some
712 influences from the sea are felt, although as in core CS22 a taphonomical impact is
713 very important. Below 756 cm, the assemblages of zones 18D-1 and 2 are brackish-
714 Pontocaspian, with significant reworking in zone 18D-1 both in dinocysts and in
715 pollen.

716 The group of dinocysts reflecting warm SST (Fig. 4 and 7) is especially
717 abundant in zone 18-D3. The presence of *B. tepikiense*, as in the CS22 core,
718 indicates seasonal temperature contrast at that time.

719 Two large peaks of *L. machaerophorum* are noted just above a hiatus, i.e. at
720 the base of zone 18D-3 and at the base of zone 18D-5b. After the transition from
721 zone 18D-2 to 3, a peak of cysts of *S. trifida* is also present. Both taxa are signs of
722 nutrient enhancement.

723 The P/D ratio fluctuates throughout the record. One may note however high
724 values in subzone 18-D1a and at the base of zone 18-D4. The values are especially
725 low in the middle of zone 18D-3, suggesting high water levels.

726 *6.2.3 Elements of chronology*

727 Zones 18D-3 (marine taxa and low P/D) and 18D-4 (transition) reflect the MIS
728 5e high sea levels. The warm-loving taxa are present in the same zone and confirm
729 interglacial conditions as deduced from pollen analysis. However, it is likely that this
730 zone is not complete as a characteristic dinozone in core CS22 (high percentages of
731 cysts of *P. dalei* and cysts of *S. trifida*) is missing (Leroy et al., 2023).

Zones D18-1 and 2 are suggested to represent low water levels and, if the sequence is in continuity, glacial stage MIS 6. As a reminder, above the red-H1 hiatus, brackish conditions have previously been related to MIS 4 (Kende, 2018; Çağatay et al., 2019).

In conclusion, the chronology proposed here represents an in-depth revision of that in Çağatay et al. (2019), with especially the occurrence of a larger part of MIS 5e and of MIS 5c and fits the chronology based on geochemistry and pollen analysis proposed in Leroy et al. (2023).

6.3 Comparison of the dinocyst records within the Sea of Marmara and to the Black Sea

6.3.1 Diversity

The dinocyst assemblages are similar in core CS22 and core CS18, with slightly more marine taxa in CS22 and brackish-Pontocaspian taxa in CS18, reflecting the difference in the extension of glacial versus interglacial periods covered in the two sequences (Table SI3). The total number of taxa is larger in core CS18; the latter because of the long MIS 6 record. Taxa at play in core 22-GC3 in the SE Black Sea (Shumilovskikh et al., 2013) are similar to those in the two Marmara cores, although the Black Sea seems to have more heterotrophic cyst diversity and the SoM more brackish-Pontocaspian taxon diversity (Table SI3). Modern and Holocene records across the Black Sea show geographic differences in the distribution of heterotrophic taxa (Mudie et al., 2017). This may be due to variations in water turbidity, limitations to photosynthesis, or possibly competition with other phytoplankton groups. Remarkably, *S. inaequalis* and *S. trifida* are two particularities of the SoM versus the Black Sea.

6.3.2 MIS 5e

In core 22-GC3 (SE Black Sea), the transition from brackish Pontocaspian to marine conditions during MIS 5e is dated at 128 ka (Shumilovskikh et al., 2013). It is marked by an increase in productivity due to rising temperature (increased in dinocyst concentration) and by the inflow of marine waters from the Mediterranean Sea (increase in the taxon number, especially those from typical marine salinities). The change is progressive contrary to that in core CS18, underlining the possibility of a hiatus in core CS18 at the beginning of the marine phase (see the earlier taphonomy section) linked to flooding by marine waters. The subsequent peak of nutrients reconstructed from the dinocyst analysis in core CS18 is possibly due to a combination of shore erosion as sea level rose and increasing temperature. The very high percentages of cysts of *P. dalei* and *S. trifida* in zone 22D-4 find no equivalent in core CS18. The transition from marine to brackish (mixed assemblages) is made over 20 cm only within zone 22D-5, whereas it is much longer in core CS18 (zone 18D-4, 70.5 cm long). These two observations suggest other significant hiati and deeper waters in the west that were invaded quickly by saline waters.

In the middle of the marine phase, a *Pinus* zone (22P-2, 2042-1982 cm depth, and 18P-6, 621-581 cm depth) has been recognised in both cores and quantitative climatic reconstruction based on pollen proposed a cool-humid climate not suggestive of a stadial steppe (Leroy et al., 2023). Due to the presence of the warm-loving dinocysts before, during and after, this mid-Eemian phase thus has an ambiguous interpretation. A continental climate in the *Pinus* zone underlined by the presence of seasonal contrast dinocyst assemblages is nevertheless likely.

The end of the marine phase is not presented in core 22-GC3 from the Black Sea due to a turbidite, although the authors suggest that the Eemian is almost

781 complete(Wegwerth et al., 2018). The end of the marine phase may however be
782 studied in the two Marmara cores here and seems to have been progressive with a
783 period when the two types of dinoflagellate assemblages co-existed (zones 22D-5
784 and 18D-4), i.e. marine and brackish.

785 It is noteworthy to underline the peaks of *S. trifida* both at the beginning of the
786 marine phase (zone 18D-3a) and at the end of it (zone 22D-4), in both cases
787 attributed to fluctuating salinities between marine and brackish-Pontocaspian. At the
788 end of the marine period in core CS22, in addition, the high values of cysts of *P.*
789 *dalei* may be attributed to terrigenous input, probably related to water level lowering,
790 as proposed for the Holocene (Verleye et al., 2009).

791 In the Black Sea, the widely-spaced analyses on core DSDP Site 380
792 sampled a weakly marine phase as the occurrence of brackish dinocyst taxa (58%)
793 is quite substantial (Ferguson et al., 2018). A diagram from DSDP Site 379A has one
794 sample in MIS 5e (Hoyle et al., 2021). This unique spectrum shows abundance of *L.*
795 *machaerophorum* with long processes, *Spiniferites* sp. and some marine taxa. The
796 $^{87}Sr/^{86}Sr$ ratio supports a marine connection at that time (Wegwerth et al., 2014;
797 Hoyle et al., 2021). The interglacial periods in the Gulf of Corinth were generally
798 marine, as Global Ocean level is high. In the lithostratigraphic unit correlated to MIS
799 5, the surface water conditions were generally warmer as established by warm-
800 loving species similar to those found in the SoM (Fatourou et al., 2023).

801 *6.3.3 MIS 6 and 4*

802 The NMDS analysis shows that MIS 6 and MIS 4 dinocyst assemblages are
803 clearly different, although both brackish-Pontocaspian (Fig. 8), i.e. more *P. psilata*
804 and clear presence of *S. inaequalis* and *Caspidinium* in MIS 6, contrasted with more
805 *S. cruciformis* in MIS 4. Some common points are noted between the MIS 6 and MIS

4 assemblages of the current study and the MIS 3 assemblages of other Marmara cores (Mudie et al., 2004): all show a mix of dominant brackish-Pontocaspian dinocysts with some marine ones and all have low to very low cyst concentrations. In MIS 4 in the Black Sea (Shumilovskikh et al., 2014), cyst concentration is also lower than in MIS 5.

The very low cyst concentration in the SoM may be due to high sedimentation rates diluting the fossil content. Erosion is active in glacial stages, as seen by the percentages of reworked elements that are very high in the MIS 6 of core CS18 and in the MIS 4 of cores CS22 and CS18. Other investigators often do not count them, neither published them, but they are a significant indicator of erosion and inwash. Often reworking also shows proximity to shores due to low water level. The water level must have been relatively low, most likely lower than at any time in MIS 5. The brackish-Pontocaspian periods during MIS 5 are clearly different from those of MIS 6 and 4, in that the latter ones have a lot of reworking and contain abundant signs of erosion (Fig. 3, 4 and 8).

Core CS18 in the Imralı basin is not far from the North Imralı canyon that the Kocasu carved during lowstands (Çağatay et al., 2015a and b). This relative proximity to a river (if not to the shore) and submarine canyon may also explain the high amounts of reworked elements and the different taphonomy during the glacial times (Pope et al., 2022).

It is very likely that, as suggested in Hoyle et al. (2021) based on Sr ratio in the Black Sea, no marine connection occurred during the glacial periods for the SoM. Several indicators (oxygen isotopes of the Sofular Cave along the Turkish coast of the Black Sea (Badertscher et al., 2011) and Sr isotope ratio (Hoyle et al., 2021)) suggest an overflow from the Caspian Sea to the Black Sea during MIS 6.

831 Unfortunately, dinocyst assemblages cannot contribute evidence to this debate on
832 water source.

833 For MIS 6 in the SoM, a progressive, even slow, freshening after marine
834 conditions in the previous interglacial (MIS 7) was suggested on the basis of
835 divergent trends in isotopic values, i.e. $\delta^{18}O$ becomes more negative while $\delta^{13}C$
836 becomes more positive (Çağatay et al., 2019). This may explain why here the marine
837 dinocyst group is better represented in subzone 18D-1a than subzones 18D-1b and
838 c, even 18D-2. This also suggests that the base of the core may have just missed
839 the top of MIS 7. As a significant contribution of reworking of marine palynomorphs
840 (as shown here) is revealed, no marine connection would have occurred during MIS
841 6 (zones 18D-1 and 2). For that matter, at the transition from the marine phase to the
842 lake phase at MIS 5 to 4, Grall et al. (2014) and Aziz et al. (2019) suggest slope
843 failure and strong turbidity currents entraining sediment that was stored on the shelf
844 to deeper areas of the SoM, as the sea level fell. Recent investigations (modern
845 discharge and geological data) aiming at disentangling the origin of the sediment in
846 the SoM during low levels have however demonstrated that southern river input was
847 more important than suspended load through one or both straits (Hiscott et al.,
848 2021). Moreover, the latter study further estimates that river input was higher than
849 mass-wasting events and shoreface erosion. Nowadays, and most likely in the past,
850 the Kocasu is the largest southern river and it drains a large basin in NW Anatolia
851 (Kazancı et al., 2004).

852 The water levels in the Black Sea were most likely low during the cold parts of
853 MIS 6. However, three major meltwater pulses of the Eurasian icesheets occurred;
854 but it is not known if the lake level rise of the Black Sea was sufficient to cause an
855 overspill to the SoM although it is likely (Wegwerth et al., 2019). So far these pulses

cannot be seen in our record. For completeness of the record, it is noteworthy to underline that the glacials (MIS 6 and 4) in the Gulf of Corinth were generally brackish (Fatourou et al., 2023).

6.4 Sapropels

6.4.1 Surface conditions and sapropel formation

The successive sapropels deposited in SoM during MIS 5 clearly formed under three different surface water conditions (Fig. 7). MSAP-2 formed under brackish surface conditions, except briefly on a few cm within MSAP 2b. MSAP-4 developed under clearly marine surface conditions. Finally, MSAP-3 built up in a period of transition from marine to brackish surface conditions.

Although not a perfect fit, the dinocyst concentration increases in each sapropel. Admittedly dinocysts are only one part of the bloom-forming phytoplankton, diatoms being the main group. In order to appreciate the amount of other phytoplankton such as diatoms, the H/A ratio is used as an indicator of primary productivity, as heterotrophic dinoflagellate prey on diatoms (see Triantaphyllou et al., 2009; Sala-Perez et al., 2020). The results show higher H/A ratio, thus higher palaeoproductivity, during the marine phase in MIS 5e in core CS18, especially in MSAP-4 (Fig. 9). The diatom assemblages (only available for MSAP-2 in core CS22) are freshwater-brackish. This H/A ratio is low in MSAP-2b, suggesting low productivity.

The various origins of the successive sapropel formation in the SoM, the decreasing surface salinities and the decrease of the oxic condition at bottom over MIS 5 may be the reason why reconstructed palaeoproductivity based on the H/A

879 ratio is clearly only higher in MSAP-4 corresponding to the warm conditions of the
880 early MIS 5e).

881 *6.4.2 Bottom conditions and sapropel formation*

882 In core CS22 below MSAP-3, the gradual shift of foraminifera assemblages,
883 starting with genera needing oxic conditions towards suboxic-tolerant genera, is an
884 effect of oxygen loss caused by the formation of water column stratification and
885 organic matter mineralisation (Fig. 9). It is worth noting that the occurrence of
886 foraminifera linings is only in the marine period. Accordingly in the marine phase of
887 core CS22, the linings occur from the core base and stop at the beginning of the
888 sapropel MSAP-3 at 1920 cm. Their occurrence is similar to that of the foraminifera
889 shells (Fig. 9).

890 In contrast, in core CS18, foraminifer linings are present at 725.5-605.5 and
891 564.5-524.5 cm depth, thus in sapropels MSAP-4 and 3. Moreover foraminifer shell
892 distribution (Çağatay et al., 2019) (Fig. 9) is like that for the linings, although
893 somewhat shorter. In core CS18, shells are found in the first part of MSAP-4 and
894 between MSAP-4 and 3.

895 This foraminifera distribution in the sapropels is therefore questioning the
896 existence of full anoxia in MSAP-4 (core CS18) and in part of MSAP-3 (mostly in
897 core CS18, no foraminifera in core CS22). For MSAP-2, it is unclear whether the
898 water remained sufficiently high saline for benthic foraminifera to live regardless of
899 oxygen availability.

900 *6.4.3 Sapropel trigger in the Sea of Marmara*

901 Combining the information from bottom and surface conditions (especially
902 dinocysts, foraminifera shells and organic linings), it may be shown that the four

Marmara sapropels (4, 3, 2b and 2a) clearly formed over times with decreasing marine influence and increasing bottom water stagnation. Moreover, they are different from each other. Only MSAP-2 may have had fully anoxic conditions during the whole sapropel time.

The difference between the two cores may be possibly explained by the shallower position of core CS18 in comparison to core CS22. The water depth difference is 260 m, adding another c. 14 m (at the end of MSAP-3) due to core depth difference, thus a total of c. 274 m difference (Fig. 9). The location of the shallower core CS 18 would make it harder to fall within the depths affected by full anoxia and would justify the occurrence of foraminifera in MSAP-4 and 3 in a dysoxic area. Our results also show that the anoxia did not rise up to 291 m water depth. In the east Mediterranean Sea, sporadic occurrences of foraminifers have been reported in sapropels S5 (MIS5e) and S6 (MIS 6e) and, more importantly, benthic foraminifers show a progressive development of dysoxic conditions before sapropel deposition (Schmiedl et al., 2013), that we also observe before MSAP-3. It is also interesting to note that, during MSAP-1 (Holocene), suboxic conditions extended over the shelf to depths of -75 m (Çağatay et al., 2009).

The Marmara sapropels occur during warm periods, evidenced in the current joint pollen-dinocyst investigation i.e. Eemian, Saint-Germain I and II, which more likely facilitated algal blooms. Consequently, the proposed correlation between the Marmara sapropels and the Mediterranean sapropels becomes: MSAP-4 – S5, MSAP-3 – not correlatable, MSAP 2b – S4 and MSAP-2a – S3 (Fig. 9), based on ages (Grant et al., 2016). The Marmara sapropels do not seem to be preconditioned by astronomical forcing the same way as for the Mediterranean ones (Rohling et al., 2015; Grant et al., 2016). A specific trigger mechanism in the SoM, as in the Black

928 Sea, is an inflow of marine water causing water column stratification (Çağatay et al.,
929 2009).

930 ## 6.5 Terrestrial and marine transitions in the Marmara and the Black seas

931 Understanding the facies transitions in the SoM or Lake requires taking into
932 account the hydrodynamic processes and how they control sediment deposition and
933 erosion in the Bosphorus and the Dardanelles Straits. The net outflow from the Black
934 Sea to the Sea of Marmara is governed by river inputs to the Black Sea and
935 evaporation/precipitation (Dubinin and Dubinina, 2014). When the water budget of
936 the Black Sea is positive, it will inevitably overspill into the SoM and then most likely
937 into the Mediterranean Sea as the SoM has a comparatively small surface area for
938 evaporation. On the other hand, the occurrence of a counter current of sea water
939 from the Mediterranean Sea to the SoM when sea level is above the Dardanelles
940 Strait and to the SoM to the Black Sea when sea level is above the Bosphorus Sill
941 cannot be taken for granted. For instance, in the present day with a sill depth of -35
942 m in the Bosphorus Strait, the seawater bottom current is blocked when the surface
943 current exceeds 30,000 $m^3.s^{-1}$ (Sannino et al., 2017). This situation occurs during
944 transient events in the present conditions, but more generally the hydrodynamics of
945 the straigs implies that the influx of seawater is a function of water depth at the sill
946 and of the freshwater outflow, which is in turn governed by river inputs and
947 evaporation/precipitation. Moreover, in steady state, the only way out for seawater
948 entering the Dardanelles Strait is by mixing with the fresher surface water layer in the
949 SoM or in the Black Sea. In the present day, and considering yearly averages, the
950 bottom current flux through the Dardanelles Strait is only about 12 % larger than the
951 bottom current flux through the Bosphorus Strait (Beşiktepe et al., 1994). It follows
952 that the halt of northward flux through the Bosphorus Strait would also greatly reduce

953 the seawater flux into the SoM and thus increase the residence time of the SoM
954 bottom water. The residence time of deep water in the SoM varies from two years in
955 the Tekirdag and the Central Basin to 10-20 years in Çınarcık Basin (Beşiktepe et
956 al., 1994), and this causes an eastward decrease of oxygen concentration from 60 to
957 8 μmol l^{-1} (Henry et al., 2007). Increasing the residence time will further reduce
958 oxygen content, which may in turn favour sapropel deposition.
959 Variations of sill elevation depend not only on sea level, but also on tectonic
960 movements, erosion and sedimentation. The shores of the Dardanelles Strait were
961 uplifting at a rate estimated in the 0.25-0.75 mm yr^{-1} range (Yaltırak et al., 2002).
962 This may suggest that the level of the sill has risen with time. However, the
963 Dardanelles Strait is at least in part structurally controlled (Yaltırak et al., 2000;
964 Gökaşan et al., 2008). Active faults, along part of its shore, may locally cause
965 subsidence of the channel floor. Two sedimentary units were deposited on an
966 erosional surface cutting through Miocene and Pliocene sediments. Their geometry
967 gives clear indications on the erosion and sedimentation processes (Gökaşan et al.,
968 2008). The lower unit is thickest (up to 80 m) at the mouths of rivers discharging in
969 the Dardanelles Strait where they formed deltas that were subsequently incised. The
970 upper unit is composed of Holocene sediment drifts that are thickest where the
971 channel is wide and are incised by the active bottom current in the narrow parts. It
972 thus appears that the strength of the bottom current in the Dardanelles Strait, which
973 is in the present-day conditions controlled by the dynamics of the Bosphorus Strait,
974 redistributes sediments and prevents clogging of the channel. All the above
975 observations and reasoning leads to hypothesize that the interruption of the
976 northward flux through the Bosphorus Strait leads to the restriction of the
977 Dardanelles channel by deltas forming at the mouths of local rivers. In the

Dardanelles Strait, the current sill depth is defined by the top of Unit I at -65 m while the basement sill is at -85 m. In the Bosphorus Strait, the present-day sill depth is at -35 m while the basement sill is at -70 m (Çağatay et al., 2009).

In core CS18, the brackish to marine transition occurs still within the Saalian Glacial (c. MIS 6), i.e. before the development of the thermophilic vegetation of the Eemian Interglacial. Moreover, the end of the marine phase occurs before the end of Eemian Interglacial in both cores. This offset is in line with the observation that the Eemian Interglacial and the MIS 5e are not exactly synchronous, with the Global Ocean level rising first, followed by vegetation changes (Shackleton et al., 2003).

In the SE Black Sea (core 22-GC3), the marine influence however starts only at 128 ka (or 815.5 cm depth) between the *Quercus-robur*-type zone (22GC-E1) and the *Juniperus* zone (22GC-E2), i.e. well into the interglacial (Shumilovskikh et al., 2013); whereas here in core CS18 it starts earlier at 756 cm depth, i.e. in the middle of zone 18P-2 dominated by *Artemisia* and that is probably still part of the Saalian Glacial (Fig. 9). Although a large difference between the SoM and the Black Sea palynological diagrams, this can be explained by the marine inflow that has first to penetrate the SoM from the Aegean Sea and cross two sills, before reaching the Black Sea. For comparison, a delay of 4-6 ka has been observed for the Lateglacial-Holocene, with a marine incursion in the SoM starting at 14.7 ka followed by progressive salinisation with a facies transition defined at 12.6 ka (Vidal et al., 2010; Çağatay et al., 2015) and in the Black Sea at 8.9-8.3 ka (Shumilovskikh et al., 2013; Mudie et al., 2014; Yakupoğlu et al., 2022). This lag has been explained by the difference in sill depth between the Bosphorus and the Dardanelles Straigs, the Bosphorus one being close to its present-day level (-35 m) at the time of reconnection and the Dardanelles one being somewhat deeper (-75 ± 5 m) than its

present-day level. The situation during the MIS 6 to 5 transition may have been similar with a Bosphorus Strait at about -40 m (Çağatay et al., 2019). The early marine incursion in the SoM at the end of MIS stage 6 indicates that the Dardanelles sill depth was also deeper at that time.

A new result from the present study that remains to be explained is the prevalence of brackish Ponto-Caspian conditions in surface water during the later phases of MIS 5 at times when sea level was well above the present-day Dardanelles sill level (Fig. 9). The explanation we propose is that the Bosphorus northward flow was first decreased then interrupted as sea level started decreasing before the end of MIS 5e, and that resulted in a progressive reduction of seawater inflow through the Dardanelles Strait and a silting up. This eventually enabled the sediment filling of the channel by local rivers, further limiting marine input. A decreased oxygen availability in the marine deep waters, as indicated by foraminifer assemblages, is observed. Low and/or episodic sea-water inputs during the later part of MIS 5 may have maintained stratified conditions in the SoM with low salinity surface waters and nearly anoxic bottom water of intermediate salinity. Sea level drop during MIS 5d and 5b presumably interrupted the marine inflow, lowering the vertical salinity contrast and allowing better oxygenation of the deep waters. During the following glacial lowstands (MIS 4-3-2), the Marmara lake remained isolated and outflow (either permanent or episodic) may have incised the sedimentary deposits to allow reconnection at ≈-75 m at the end of the glaciation.

The $\delta\,^{18}O$ of the well-dated Sofular stalagmite record reflect the composition of the Black Sea surface waters by way of evaporation and moisture availability (Badertscher et al., 2011) (Fig. 1). These authors propose one clear period of connection between the Black Sea and the Mediterranean Sea at roughly MIS 5e

based on a threshold of -8.5± 1‰ $\delta^{18}O$ values. The next period below that threshold is at MIS 5c and the data also suggest connection but for a shorter period. The last period at MIS 5a would not have led to sufficiently high water levels to allow flowing of the Mediterranean marine waters into the Black Sea. This fits rather well our results in the SoM, with a full surface water connection at MIS 5e when global sea level reached 8 m above sea level, a marine incursion affecting surface waters during MIS 5c when global sea level reached 24 m below sea level and no incursion during MIS 5a when global sea level reached only 28 m below sea level (Rohling et al., 2021).

7 Conclusions

The results of this investigation have shown the widely changing states of the Sea of Marmara during the MIS 6 and 5, implying vastly changing connexions with the Pontocaspian basin and the Global Ocean.

From the methodological point of view, as for the Caspian Sea (Leroy et al., 2013, 2014) when using the palynological method at large, it is essential to study separately and objectively the terrestrial conditions and the aquatic ones. A comparison of the two approaches may then clearly demonstrate if the changes are synchronous or not, and if different forcing factors are at play.

As demonstrated for the Iberian margin by pollen and isotopic analyses (Shackleton et al., 2003), the Eemian starts and finishes respectively after the start and after the end of MIS 5e high levels. The same offset can be demonstrated here in this joint pollen - dinocyst study.

The combination of the two sequences, CS22 and CS18, following the chronology proposed in Leroy et al. (2023), allows highlighting one main marine

phase corresponding to MIS 5e and a minor one in MIS 5c. The rest of the record is brackish-Pontocaspian although with some differences across the sequence (e.g. MIS 6 versus MIS 4). Based on vegetation and climatic data allowing linking the records, a delay in the marine influence between SoM and SE Black Sea is observed, perhaps due to the closure of the Bosphorus Sill and its late opening or a different sill height.

The current water level reconstruction in MIS 5 corresponds well to the Global Ocean level curve and Black Sea salinity reconstructions, both indicating high stands that become progressively lower and thus decreasing connections between the Black Sea and the SoM.

The four sapropels (MSAP-4, 3, 2a and 2b) formed under very different surface water conditions ranging from marine to brackish-Pontocaspian, but always under a warm climate. Moreover, the shallower site in the east (Imralı basin) does not form as often full anoxia than the western and deeper site.

In the future, it would be interesting to apply palynological investigations (pollen and dinocysts) on long cores on both sides of the Bosphorus Strait to define better for example the timing difference for the marine reconnection at the boundary MIS 6-5.

Acknowledgements

We are grateful to Jennifer Bradley and Luke Glascott at the University of Liverpool (UK) and Dahvya Belkacem at IMBE (Aix-en-Provence, France) for palynological extraction in the pollen laboratories. Cores were taken during the MARSITECRUISE of Ifremer/Genavir R.V. Pourquoi Pas?, within the framework of MARSITE FP7 EU Project (grant agreement no: 308417). Thanks are due to N.

Çağatay, K. Eriş and N. Yakupoğlu from ITU (Turkey) who gave access to core CS18 for sampling and contributed to the improvement of this publication owing to intensive discussions over the years. Part of this work has been supported by Bilateral ANR/TÜBITAK collaborative research project MAREGAMI (ANR-16-CE03-0010-02) and Tubitak Project (116Y371). We are grateful to the reviewers for their constructive comments.

Data availability

The dinocyst data are available in PANGEA.

References

Aloisi, G., Soulet, G., Henry, P., Wallmann, K., Sauvestre, R., Vallet-Coulomb, C., Lécuyer, C., Bard, E., 2015. Freshening of the Marmara Sea prior to its post-glacial reconnection to the Mediterranean Sea. Earth and Planetary Science Letters 413, 176-185.

Aydoğdu, A., Pinardi, N., Özsoy, E., Danabasoglu, G., Gürses, O, Karspeck, A., 2018. Circulation of the Turkish Straits System under interannual atmospheric forcing. Ocean Sci. 14, 999–1019.

Aziz, S., McHugh, C.M., Ryan, W.B.F., Henry, P., Kende, J., Delligatti, M., Tachikawa, K., 2019. New insights into the rapid transformation of the sea into a lake, Marmara Sea, Turkey. AGU abstract. https://ui.adsabs.harvard.edu/abs/2019AGUFMPP21D1650A/abstract

1097 Badertscher, S., Fleitmann, D., Cheng, H., Edwards, R.L., Göktürk, O.M., Zumbühl,
1098 A., Leuenberger, M., Tüysüz, O., 2011. Pleistocene water intrusions from the
1099 Mediterranean and Caspian seas into the Black Sea. Nat. Geosci. 4, 236–239.
1100 Bahr, A., Arz, H. W., Lamy, F., Wefer, G., 2006. Late glacial to Holocene
1101 paleoenvironmental evolution of the Black Sea, reconstructed with stable oxygen
1102 isotope records obtained on ostracod shells. Earth Planet. Sci. Lett., 241, 863–
1103 875, https://doi.org/10.1016/j.epsl.2005.10.036.
1104 Balkis, N., Balci, M., Giannakourou, A., Venetsanopoulou, A., Mudie, P., 2016.
1105 Dinoflagellate resting cysts in recent marine sediments from the Gulf of Gemlik
1106 (Marmara Sea, Turkey) and seasonal harmful algal blooms. Phycologia 55, 2,
1107 187–209
1108 Bard, E., Jouannic, C, Hamelin, B., Pirazzoli, P., Arnold, M., Faure, G.,
1109 Sumosusastro, P., Syaefudin, 1996. Pleistocene sea levels and tectonic uplift
1110 based on dating of corals from Sumba Island, Indonesia. Geoph. Res. Lett. 23,
1111 12, 1473-1476.
1112 Bennett, K., 2007. Psimpoll and Pscomb Programs for Plotting and Analysis. Version
1113 Psimpoll 4.27. http://chrono.qub.ac.uk/psimpoll/psimpoll.html (accessed 27 May
1114 2020).
1115 Beşiktepe, S.T., Sur, H.I., Özsoy, E., Latif, M.A., Oğuz, T., Ünlüata, Ü., 1994. The
1116 circulation and hydrography of the Marmara Sea. Prog. Oceanogr. 34, 285–334.
1117 Bradley, L.R., Marret, F., Mudie, P.J. et al., 2012. Constraining Holocene sea-
1118 surface conditions in the south-western Black Sea using dinoflagellate cysts.
1119 Journal of Quaternary Science 27, 835–843.
1120 Bravo, I., Figueroa, R.I., 2014. Towards an ecological understanding of dinoflagellate
1121 cyst functions. Microorganisms, 2, 11–32.

1122 Çağatay, M.N, Görür, N., Algan, A, Eastoe, C.J., Tchapalyga, A., Ongan, D., Kuhn,
1123 T, Kuşcu, İ., 2000. Late Glacial-Holocene palaeoceanography of the Sea of
1124 Marmara: timing of connections with the Mediterranean and the Black
1125 Sea. Marine Geology 167, 191-206.
1126 Çağatay, M.N., Eriş, K., Ryan, W.B.F., Sancar, Ü., Polonia, A., Akçer, S., Biltekin, D.,
1127 Gasperini, L., Görür, N., Lericolais, G., Bard, E., 2009. Late Pleistocene–
1128 Holocene evolution of the northern shelf of the Sea of Marmara. Marine Geology
1129 265, 87–100.
1130 Çağatay, M.N., Wulf, S., Sancar, Ü., Özmaral, A., Vidal, L., Henry, P., Gasperini, L.,
1131 2015a. The tephra record from the Sea of Marmara for the last ca. 70 ka and its
1132 palaeoceanographic implications. Mar. Geol. 361, 96-110.
1133 Çağatay, M.N., Uçarkuş, G., Eriş, K.K, Henry, P., Gasperini, L., Polonia, P., 2015b.
1134 Submarine canyons of the Sea of Marmara. In CIESM Monograph 47 [F. Briand
1135 ed.] Submarine canyon dynamics in the Mediterranean and tributary seas- An
1136 integrated geological, oceanographic and biological perspective, pp. 123- 135.
1137 CIESM Publisher, Monaco.
1138 Çağatay, M.N., Eriş, K.K., Makaroglu, Ö., Yakuboğlu, N., Henry, P., Leroy, S.,
1139 Uçarkuş, G., Sakınç, M., Yalamaz, B., Bozyiğit, C., Kende, J., 2019. The Sea of
1140 Marmara during Marine Isotope Stages 5 and 6. Quat. Sc. Rev. 220, 124-141.
1141 Çağatay, M.N., Eriş, K.K., Erdem, Z., 2022. Morphology and Late Pleistocene-
1142 Holocene Sedimentation of the Strait of İstanbul (Bosphorus): A review. In: Rossi,
1143 V. M., Longhitano, S., Olariu, C. and Chiocci, F. (eds) Straits and Seaways:
1144 Controls, Processes and Implications in Modern and Ancient Systems. Geological
1145 Society, London, Special Publications, 523, https://doi.org/10.1144/SP523-2021-
1146 48.

1147 Cheddadi, R., Rossignol-Strick, M., 1995. Improved preservation of organic matter
1148 and pollen in eastern Mediterranean sapropels. Paleoceanography 10, 2, 301-
1149 309.
1150 Chepalyga, A.L., 2007. The late glacial great flood in the Ponto-Caspian basin. in:
1151 Yanko-Hombach, V., Gilbert, A.S., Panin, N., Dolukhanov, P.M. (Eds), The Black
1152 Sea Flood Question. Springer, pp. 119-148
1153 Clarke, K.R., Gorley, R.N., 2015. PRIMER v7: User Manual/Tutorial. PRIMER-E,
1154 Plymouth (296 pp.).
1155 Cornuault, M., Vidal, L., Tachikawa, K., Licari, L., Rouaud, G., Sonzogni, C., Revel,
1156 M., 2016. Deep water circulation within the eastern Mediterranean Sea over the
1157 last 95 kyr: New insights from stable isotopes and benthic foraminiferal
1158 assemblages. Palaeogeography, Palaeoclimatology, Palaeoecology 459, 1–14.
1159 De Lange, G. J., Thomson, J., Reitz, A., Slomp, C. P., Speranza Principato, M.,
1160 Erba, E., and Corselli, C., 2008. Synchronous basin-wide formation and redox-
1161 controlled preservation of a Mediterranean sapropel. Nat. Geosci., 1, 606–610,
1162 https://doi.org/10.1038/ngeo283.
1163 de Vernal, A., 2009. Marine palynology. IOP Conf. Ser.: Earth Environ. Sci. 5
1164 012002.
1165 de Vernal, A., Marret, F., 2007. Organic-Walled Dinoflagellate Cysts: Tracers of Sea-
1166 Surface Conditions. Development in Marine Geology 1, 371-408.
1167 de Vernal, A., Radi, T., Zaragosi, S., Van Nieuwenhove, N., Rochon, A., Allan, E.,
1168 De Schepper, S., Eynaud, F., Head, M.J., Limoges, A., Londeix, L., Marret, F.,
1169 Matthiessen, J., Penaud, A., Pospelova, V., Price, A., Richerol, T. 2020.
1170 Distribution of common modern dinoflagellate cyst taxa in surface sediments of

the Northern Hemisphere in relation to environmental parameters: The new n=1968 database. Marine Micropaleontology, art. no. 101796.

Dubinin, A. V. and Dubinina, E. O., 2014. Isotope composition of oxygen and hydrogen in the Black Sea waters as a result of the dynamics of water masses, Oceanology, 54, 713–729, https://doi.org/10.1134/S0001437014050038.

Eriş, K.K., Ryan, W.B.F, Çağatay, M.N., Sancar, U., Lericolais, G., Menot, G., Bard, E., 2007. The timing and evolution of the post-glacial transgression across the Sea of Marmara shelf south of İstanbul. Marine Geology 243, 1-4, 57-76.

Eriş, K.K., Çağatay, M.N., Akçer, S., Casperini, L., Mart, Y., 2011. Late glacial to Holocene sea-level changes in the Sea of Marmara: new evidence from high-resolution seismics and core studies.Geo-Marine Letters 31, 1, 1-18.

Fatourou, E., Kaftzidou, A., Marret, F., Panagiotopoulos, K., Kouli, K., 2023. Late Quaternary Ponto-Caspian dinoflagellate cyst assemblages from the Gulf of Corinth, Central Greece (eastern Mediterranean Sea). Marine Micropal. 179, 102211.

Ferguson, S., Warny, S., Escarguel, G., Mudie, P.J., 2018. MIS 5e1 dinoflagellate cyst analyses and morphometric evaluation of *Galeacysta etrusca* and *Spiniferites cruciformis* in southwestern Black Sea. Quaternary International 465, 117-129.

Géli, L., Ruffine, L., Henry, P., Cağatay, M.N., 2014. MARSITECRUISE cruise, RV Pourquoi pas ?, https://doi.org/10.17600/14000500

Gökaşan, E., Ergin, M., Özyalvaç, M., Sur, H.I., Tur, H., Görüm, T., Ustaömer, T., Batuk, F.G., Alp, H., Birkan, H., Türker, A., Gezgin, E., Özturan, M., 2008. Factors controlling the morphological evolution of the Çanakkale Strait (Dardanelles, Turkey). Geo-Mar. Lett. 28,107–129.

1195 Gökaşan E., Tur, H., Ecevitoglu, B., Görüm, T., Türker, A., Tok, B., Çaglak, F.,
1196 Birkan, H., Simşek, M., 2005. Evidence and implications of massive erosion along
1197 the Strait of Istanbul (Bosphorus). Geo-Mar. Lett. 25, 324–342.
1198 Grall, C., Henry, P., Thomas, Y., Westbrook, G. K., Çağatay, M. N., Marsset, B.,
1199 Saritas, H., Çifçi, G., and Géli, L., 2013. Slip rate estimation along the western
1200 segment of the main Marmara fault over the last 405-490 ka by correlating mass
1201 transport deposits, Tectonics, 32, 1587–1601,
1202 https://doi.org/10.1002/2012TC003255.
1203 Grall, C., Henry, P., Westbrook, G.K., Cagatay, MN, Thomas, Y., Marsset, B.,
1204 Borschneck, D., Saritas, H., Cifçi, G., Géli, L., 2014. Mass transport deposits
1205 periodicity related to glacial cycles and marine-lacustrine transitions on a ponded
1206 basin of the Sea of Marmara (Turkey) over the last 500 ka. Chapter 53. In:
1207 Krastel, S. et al. (eds) Submarine mass movement and their consequences.
1208 Advances in Natural and Technological Hazards Research 37, Springer
1209 International Publishing Switzerland, pp. 595-603.
1210 Grant, K.M., Grimm, R., Mikolajewicz, U., Marino, G., Ziegler, M., Rohling, E.J.,
1211 2016. The timing of Mediterranean sapropel deposition relative to insolation, sea-
1212 level and African monsoon changes. Quaternary Science Reviews 140, 125-141.
1213 Grimm, R., Maier-Reimer, E., Mikolajewicz, U., Schmiedl, G., Müller-Navarra, K.,
1214 Adloff, F., Grant, K. M., Ziegler, M., Lourens, L. J., and Emeis, K.-C., 2015. Late
1215 glacial initiation of Holocene eastern Mediterranean sapropel formation, Nat.
1216 Commun., 6, 7099, https://doi.org/10.1038/ncomms8099.
1217 Head, M.J., Lewis, J., de Vernal A., 2006. The cyst of the calcareous dinoflagellate
1218 *Scrippsiella trifida*: resolving the fossil record of its organic wall with that of
1219 *Alexandrium tamarense*. Journal of Paleontology 80, 1, 1-18.

1220 Henry, P., Şengör, A.M.C., Çağatay, M.N., 2007. MARNAUT cruise, RV L'Atalante.
1221 https://doi.org/10.17600/7010070.
1222 Hiscott, R.N., Aksu, A.E., Yaltırak, C., 2021. The uppermost Pleistocene–Holocene
1223 mud drape across the Marmara Sea: Quantification of detrital supply from
1224 southern Marmara rivers. Sedimentary Geology 415, 105851.
1225 Hoyle, T., Bista, D., Flecker, R., Krijgsman, W., Sangiorgi, F., 2021. Climate-driven
1226 connectivity changes of the Black Sea since 430 ka: Testing a dual palynological
1227 and geochemical approach. Palaeogeography, Palaeoclimatology, Palaeoecology
1228 561, 110069.
1229 Kaminski, M.A., Aksu, A., Box, M., Hiscott, R., Filipescu, S., Al-Salameen, M. 2002.
1230 Late Glacial to Holocene benthic foraminifera in the Marmara Sea: implications for
1231 Black Sea-Mediterranean Sea connections following the last deglaciation. Marine
1232 Geology 190: 165-202.
1233 Kirci-Elmas, E.K., Algan, O., Öngen, İ.Ö., Struck, U., Altenbach, A.V., Sagular, E.K.,
1234 Nazik, A., 2008. Palaeoenvironmental investigation of sapropelic sediments from
1235 the Marmara Sea: A biostratigraphic approach to palaeoceanographic history
1236 during the last glacial-Holocene. Turkish Journal of Earth Sciences 17, 129-168.
1237 Karabanov, E.B, Prokopenko, A.A., Williams, D.F., Khursevich, G.K., 2000. Evidence
1238 for mid-Eemian cooling in continental climatic record from Lake Baikal. Journal of
1239 Paleolimnology 23, 365–371.
1240 Kazancı, N., Leroy, S., Ileri, Ö., Emre, O., Kibar, M., Öncel, S., 2004. Late Holocene
1241 erosion in NW Anatolia from sediments of Lake Manyas, Lake Ulubat and the
1242 southern shelf of the Marmara Sea, Turkey. Catena 57, 277-308.
1243 Kende, J., 2018. Tectonique et hydrologie en mer de Marmara : Histoire de
1244 l’ouverture de la mer de Marmara et reconstitution de la réponse hydrologique aux

1245 variations climatiques depuis le dernier interglaciaire. Thèse de doctorat, Aix-
1246 Marseille Université. 18 pp. available at https://hal.science/tel-01907260
1247 Koeling, M., Webster, J.M., Camoin, G., Iryu, Y., Bard, E., Seard, C., 2009. SEALEX
1248 — Internal reef chronology and virtual drill logs from a spreadsheet-based reef
1249 growth model. Glob. Planet. Ch. 66, 149-159.
1250 Kotthoff, U., Pross, J., Müller, U. C., Peyron, O., Schmiedl, G., Schulz, H., Bordon,
1251 A., 2008. Climate dynamics in the borderlands of the Aegean Sea during
1252 formation of sapropel S1 deduced from a marine pollen record. Quaternary
1253 Science Reviews 27, 832–845.
1254 Leroy, S.A.G., Marret, F., Giralt, S., Bulatov, S. A., 2006. Natural and anthropogenic
1255 rapid changes in the Kara-Bogaz Gol over the last two centuries by palynological
1256 analyses. Quaternary International 150, 52-70.
1257 Leroy, S.A.G., 2010, Palaeoenvironmental and palaeoclimatic changes in the
1258 Caspian Sea region since the Lateglacial from palynological analyses of marine
1259 sediment cores. Geography, Environment, Sustainability, Faculty of Geography
1260 of Lomonosov Moscow State University and by the Institute of Geography of
1261 RAS. 2, 32-41.
1262 Leroy, S.A.G., Tudryn, A., Chalié, F., López-Merino, L., Gasse, F., 2013. From the
1263 Allerød to the mid-Holocene: palynological evidence from the south basin of the
1264 Caspian Sea. Quaternary Science Reviews 78, 77-97.
1265 Leroy, S.A.G., López-Merino, L., Tudryn, A., Chalié, F., Gasse, F., 2014. Late
1266 Pleistocene and Holocene palaeoenvironments in and around the Middle
1267 Caspian Basin as reconstructed from a deep-sea core. Quaternary Science
1268 Reviews 101, 91-110.

1269 Leroy, S.A.G., Lahijani, H., Crétaux, J.-F., Aladin, N., Plotnikov, I., 2020. Past and
1270 current changes in the largest lake of the world: The Caspian Sea. in: Mischke,
1271 S. (Ed.), Large Asian lakes in a changing world. Springer, pp. 65-107.
1272 Leroy, S.A.G., Henry, P., Peyron, O., Rostek, F., Kende, J., Bard, E tachikawa, K..,
1273 2023. Palynology, palaeoclimate and chronology from the Saalian Glacial to
1274 Saint-Germain II Interstadial from two long cores at the limit between the
1275 Mediterranean and Euxinian regions. Quat Sc Rev
1276 Lisiecki, L.E., Raymo, M.E., 2005. A Pliocene-Pleistocene stack of 57 globally
1277 distributed benthic $\delta^{18}O$ records. Paleoceanography, 20, PA1003
1278 Londeix, L., Herreyre, Y., Turon, J.-L., Fletcher, W., 2009. Last Glacial to Holocene
1279 hydrology of the Marmara Sea inferred from a dinoflagellate cyst record.
1280 Review of Palaeobotany and Palynology 158, 52–71.
1281 Margalef, R., 1958. Information theory in ecology. Gen. Syst. 3, 36–71.
1282 Marlowe, I. T., Brassell, S. C., Eglinton, G., and Green, J. C., 1984. Long chain
1283 unsaturated ketones and esters in living algae and marine sediments, Org.
1284 Geochem., 6, 135–141, https://doi.org/10.1016/0146-6380(84)90034-2.
1285 Marret, F., Zonneveld, K.A.F., 2003. Atlas of modern organic-walled dinoflagellate
1286 cyst distribution. Review of Palaeobotany and Palynology 125, 1–200.
1287 Marret, F., Leroy, S., Chalié, F., Gasse, F., 2004. New organic-walled dinoflagellate
1288 cysts from recent sediments of central Asian seas. Rev. Palaeobot. Palynol.
1289 129, 1–20.
1290 Marret, F., Mudie, P., Aksu, A., Hiscott, R.N., 2009. A Holocene dinocyst of a two-
1291 step transformation of the Neoeuxinian brackish water lake into the Black Sea.
1292 Quaternary International 197, 72-86.

1293 Marret, F., Bradley, L.R., Tarasov, P.E., Ivanova, E.V., Zenina, M.A., Murdmaa, I.O.,
1294 2019. The Holocene history of the NE Black Sea and surrounding areas: An
1295 integrated record of marine and terrestrial palaeoenvironmental change. The
1296 Holocene 1–14.
1297 Marret, F., Bradley, L., de Vernal, A., Hardy, W., Kim, S.Y., Mudie, P., Penaud, A.,
1298 Pospelova, V., Price, A.M., Radi, T., Rochon, A., 2020. From bi-polar to
1299 regional distribution of modern dinoflagellate cysts, an overview of their
1300 biogeography. Mar Micropal 159, 101753.
1301 McCarthy, F.M.G., Mudie, P.J., 1998. Oceanic pollen transport and pollen: dinocyst
1302 ratios as markers of late Cenozoic sea level change and sediment transport.
1303 Palaeogeography, Palaeoclimatology, Palaeoecology 138, 187-206.
1304 Mertens, K. Ribeiro, S., Bouimetarhan, I., Caner, H., Combourieu-Nebout, N., Dale,
1305 B., de Vernal, A., Ellegaard, M., Filipova, M., Godhe, A., Grøsfjeld, K., Leroy, S.
1306 A. G. and co-authors, 2009. Process length variation in cysts of a
1307 dinoflagellate, *Lingulodinium machaerophorum*, in surface sediments:
1308 investigating its potential as salinity proxy. Marine Micropal 70, 54-69.
1309 Mertens, K.N., Van Nieuwenhove, N., Gurdebeke, P.R., Aydin, H., Bogus, K.,
1310 Bringué, M., Dale, B., De Schepper, S., de Vernal, A., Ellegaard, M., Grothe,
1311 A., Gu, H., Head, M.J., Heikkilä, M., Limoges, A., Londeix, L., Louwye, S.,
1312 Marret, F., Masure, E., Matsuoka, K., Mudie, P.J., Penaud, A., Pospelova, V.,
1313 Price, A.M., Ribeiro, S., Rochon, A., Sangiorgi, F., Schreck, M., Torres, V.,
1314 Uzar, S., Versteegh, G.J.M., Warny, S., Zonneveld, K., 2018. The dinoflagellate
1315 cyst genera *Achomosphaera* Evitt 1963 and *Spiniferites* Mantell 1850 in
1316 Pliocene to modern sediments: a summary of round table discussions.
1317 Palynology 42, sup1, 10-44

1318 Mudie, P.J., Aksu, A.E., Yasar, D., 2001. Late Quaternary dinocysts from the Black,
1319 Marmara and Aegean Seas: Variations in assemblages, morphology and
1320 paleosalinity. Mar. Micropal. 43, 155-178.
1321 Mudie, P.J., Rochon A., Aksu, A.E., Gillespie, H., 2002. Dinoflagellate cysts,
1322 freshwater algae and fungal spores as salinity indicators in Late Quaternary
1323 cores from Marmara and Black seas. Mar. Geol. 190, 203-231.
1324 Mudie, P.J., Rochon, A., Aksu, A.E., Gillespie, H., 2004. Late glacial, Holocene and
1325 modern dinoflagellate cyst assemblages in the Aegean–Marmara–Black Sea
1326 corridor: statistical analysis and re-interpretation of the early Holocene Noah's
1327 Flood hypothesis. Rev. Palaeobot. Palynol. 128, 1-2, 143-167.
1328 Mudie, P., Yanko-Hombach, V., Kadurin, S., 2014. The Black Sea Dating Game and
1329 Holocene Marine Transgression. Open Journal of Marine Science 4, 1-7.
1330 Mudie, P.J., Marret, F., Mertens, K., Shumilovskikh, L., Leroy, SAG, 2017. Atlas of
1331 modern dinoflagellate cyst distributions in the Black Sea Corridor, including
1332 Caspian and Aral Seas. Mar Mic 134, 1-152.
1333 Mudie, P.J., Marret, F., Gurdebeke, P.R., Hartman, J.D., Reid, P.C., 2021. Marine
1334 dinocysts, acritarchs and less well-known NPP: tintinnids, ostracod and
1335 foraminiferal linings, copepod and worm remains. Geological Society, London,
1336 Special Publications 511, SP511-2020-2055.
1337 Paillès, C., Blanc-Valleron, M.M, Poulin, M., Crémière, A., Boudouma, O., Pierre, C.,
1338 2014. A new fossil diatom, *Entomoneis calixasini*, from the Turkish Marmara
1339 Sea sediments. Diatom Research 29, 4, 411-422.
1340 Pope, E.L., et al., 2022. First source-to-sink monitoring shows dense head controls
1341 sediment flux and runout in turbidity currents. Sci. Adv. 8, eabj3220.

1342 Rohling, E.J., Marino, G., Grant, K.M., 2015. Mediterranean climate and
1343 oceanography, and the periodic development of anoxic events (sapropels).
1344 Earth Sci. Rev. 143, 62-97.
1345 Rohling, E.J., Yu, J., Heslop, D., Foster, G.L., Opdyke, B., Roberts A.P., 2021. Sea
1346 level and deep-sea temperature reconstructions suggest quasi-stable states
1347 and critical transitions over the past 40 million years. Sci. Adv. 2021; 7.
1348 Sala-Pérez, M., Lattuada, M., Flecker, R., Anesio, A., Leroy, S.A.G.,
1349 2020. Dinoflagellate cyst assemblages as indicators of environmental
1350 conditions and shipping activities in coastal areas of the Black and Caspian
1351 Seas. Regional Studies in Marine Science 38, 101472.
1352 Sannino, G., Sözer, A., Özsoy, E., 2017. A high-resolution modelling study of the
1353 Turkish Straits System. Ocean Dynamics, 67, 397–432,
1354 https://doi.org/10.1007/s10236-017-1039-2.
1355 Schmiedl, G., Mitschele, A., Beck, S., Emeis, K.-C., Hemleben, C., Schulz, H.,
1356 Sperling, M., Weldeab, S., 2003. Benthic foraminiferal record of ecosystem
1357 variability in the eastern Mediterranean Sea during times of sapropel S5 and S6
1358 deposition. Palaeogeography, Palaeoclimatology, Palaeoecology 190, 139-164.
1359 Shackleton, N.J., Sanchez-Goñi, M. F., Pailler, D., Lancelot, Y., 2003. Marine
1360 Isotope Substage 5e and the Eemian Interglacial. Global and Planetary
1361 Change 36, 151-155.
1362 Shumilovskikh, L.S., Fleitmann, D., Nowaczyk, N.R., Behling, H., Marret, F.,
1363 Wegwerth, A., Arz, H.W., 2014. Orbital- and millennial-scale environmental
1364 changes between 64 and 20 ka BP recorded in Black Sea sediments. Clim.
1365 Past 10, 939-954.

Shumilovskikh, L.S., Marret, F., Fleitmann, D., Arz, H.W., Nowaczyk, N., Behling, H., 2013. Eemian and Holocene sea-surface conditions in the southern Black Sea: Organic-walled dinoflagellate cyst record from core 22-GC3. Mar. Micropal. 101, 146-160.

Sonzogni, C., Bard, E., Rostek, F., Dollfus, D., Rosell-Melé, A., Eglinton, G., 1997. Temperature and Salinity Effects on Alkenone Ratios Measured in Surface Sediments from the Indian Ocean. Quaternary Research 47, 3, 344–355. http://doi.org/10.1006/qres.1997.1885

Sorlien, C.C., Akhun, S.D., Seeber, L., Steckler, M.S., Shillington, D.J., Kurt, H., Imren, C., 2012. Uniform basin growth over the last 500 ka, north Anatolian fault, Marmara Sea, Turkey. Tectonophysics 518, 1-16.

Sorrel, P., Popescu, S.-M., Head, M. J., Suc, J.-P., Klotz, S., Oberhänsli, H., 2006. Hydrographic development of the Aral Sea during the last 2000 years based on a quantitative analysis of dinoflagellate cysts, Palaeogeography, Palaeoclimatology, Palaeoecology 234, 304–327.

Soulet, G, Menot, G, Bayon, G, Rostek, F, Ponzevera, E, Toucanne, S, Lericolais, G, Bard, E., 2013. Abrupt drainage cycles of the Fennoscandian Ice Sheet. Proceedings of the National Academy of Sciences 110(17): 6682–7.

Soulet, G., Ménot, G., Garreta, V., Rostek, F., Zaragosi, S., Lericolais, G., and Bard, E., 2011. Black Sea “Lake” reservoir age evolution since the Last Glacial - Hydrologic and climatic implications. Earth Planet. Sci. Lett., 308, 245–258, https://doi.org/10.1016/j.epsl.2011.06.002, 2011.

Sperling, M., Schmiedl, G., Hemleben, C., Emeis, K. C., Erlenkeuser, H., and Grootes, P. M., 2003. Black Sea impact on the formation of eastern Mediterranean sapropel S1? Evidence from the Marmara Sea, Palaeogeogr.

1391 Palaeoclimatol. Palaeoecol., 190, 9–21, https://doi.org/10.1016/S0031-
1392 0182(02)00596-5.
1393 Tolun, T., Çağatay, M.N., Carrigan, W.J., 2002. Organic geochemistry and origin of
1394 Holocene sapropelic layer and associated sediments in Marmara Sea. Mar.
1395 Geol. 190, 47–60.
1396 Triantaphyllou, M.V., Antonarakou, A., Kouli, K., Dimiza, M., Kontakiotis, G.,
1397 Papanikolaou, M. D., Ziveri, P., Mortyn, P. G., Lianou, V., Lykousis, V.,
1398 Dermitzakis, M. D., 2009. Late Glacial–Holocene ecostratigraphy of the south-
1399 eastern Aegean Sea, based on plankton and pollen assemblages. Geo-Mar.
1400 Lett. 29, 249–267.
1401 Tudryn, A., Leroy, S.A.G., Toucanne, S., Gibert-Brunet, E., Tucholka, P., Lavrushin,
1402 Y.A., Dufaure, O., Miska, S., Bayon, G., 2016. The Ponto-Caspian basin as a final
1403 trap for southeastern Scandinavian ice-sheet meltwater. Quat Sci Rev 148, 29-43.
1404 Vidal, L., Ménot, G., Joly, C., Bruneton, H., Rostek, F., Çağatay, M.N., Major, C.,
1405 Bard, E., 2010. Hydrology in the Sea of Marmara during the last 23 ka:
1406 Implications for timing of Black Sea connections and sapropel deposition.
1407 Paleoceanography 25, PA1205.
1408 Wegwerth, A., Dellwig, O., Kaiser, J., Ménot, G., Bard, E., Shumilovskikh, L.,
1409 Schnetger, B., Kleinhanns, I.C., Wille, M., Arz, H.W., 2014. Meltwater events and
1410 the Mediterranean reconnection at the Saalian-Eemian transition in the Black Sea.
1411 Earth and Planetary Science Letters 404, 124-135.
1412 Wegwerth, A., Eckert, S., Dellwig, O., Schnetger, B., Severmann, S., Weyer, S.,
1413 Brüske, A., Kaiser, J., Köster, J., Arz, H.W., Brumsack, H.-J., 2018. Redox
1414 evolution during Eemian and Holocene sapropel formation in the Black Sea.
1415 Palaeogeography, Palaeoclimatology, Palaeoecology 489, 249–260.

Wegwerth, A., Dellwig, O., Wulf, S., Plessen, B., Kleinhanns, I., Nowaczyk, N.T., Jiabo, L., Arz, H.W., 2019. Major hydrological shifts in the Black Sea “Lake” in response to ice sheet collapses during MIS 6 (130-184 ka BP). Quaternary Science Reviews 219, 126-144.

Wulf, S., Çağatay, M. N., Appelt, O., Eriş, K. K., and Henry, P., 2021. Defining the Upper Nisyros Pumice (57.1 ± 1.5 ka) as new tephra isochrone for linking early MIS-3 palaeoenvironmental records in the Aegean-Black Sea gateway: New evidence from the Sea of Marmara, Quat. Sci. Rev., 274, 107285, https://doi.org/10.1016/j.quascirev.2021.107285.

Yakupoğlu, N., Henry, P., Uçarkus¸ G., Eris, K.K., Demory, F., Crouzet, C., Çağatay, M.N., 2022. Factors affecting thickness and frequency of turbidites triggered by earthquakes in Kumburgaz Basin, Sea of Marmara. Marine Geology 452, 106900.

Yaltırak, C., Alpar, B., Sakınc, M., Yüce, H., 2000. Origin of the Strait of Çanakkale (Dardanelles): regional tectonics and the Mediterranean-Marmara incursion. Mar. Geol. 164, 139-156 (with erratum 167, 189-190).

Yaltırak, C., 2002. Tectonic evolution of the Marmara Sea and its surroundings. Marine Geology 190, 493-529.

Zwiep, K.L., Hennekamp, R., Donders, T.H., van Helmond, N.A.G.M., de Lange, G.J., Sangiorgi, F., 2018. Marine productivity, water column processes and seafloor anoxia in relation to Nile discharge during sapropels S1 and S3. Quaternary Science Reviews 200, 178-190.

Zubakov, V. A., 1988. Climatostratigraphic scheme of the Black Sea Pleistocene and its correlation with the oxygen-isotope scale and glacial events, Quat. Res., 29, 1–24, https://doi.org/10.1016/0033-5894(88)90067-1.

Supplementary information

Table SI1: Benthic foraminifera census data in nine samples from core CS22

Core CS22										
benthic foraminifera census data										
	depth (cm)	1631	1632	1915	1935	1955	1975	1995	2015	2035
shallow-water species	*Ammonia parkinsoniana*			2						
	Ammonia sp					1				
	Discorbinella bertheloti							1	3	3
	Elphidium sp			1						
	Haynesina depressula			5						
	Rosalina sp						1		1	2
	Porosononion granosum			1						
hyaline bathyal species	*Amphicoryna scalaris*							1		
	Bolivinita quadrilatera						1			
	Bolivina striatula									2
	Bolivina alata				64	371	101			
	Bolivina dilatata				16	4	5			1
	Bolivina spathulata				1	2	78	9	7	2
	Bulimina aculeata					5	6	8	11	5
	Bulimina inflata					1	4	151	235	115
	Bulimina elongata				7	6	5		1	1
	Bulimina marginata				98	5	1	3	4	1
	Bulimina sp							7	2	
	Cassidulina carinata				15	2	8	32	9	
	Cassidulina obtusa									2
	Chilostomella oolina							2	3	7
	Chilostomella ovoidea					11	10	3		
	Chilostomella sp					3				
	Cibicidoides pachyderma					1	6	35	15	
	Cibicidoides pseudoungerianus							7		1
	Cibicidoides sp						1	8		2
	Dentalina sp								1	
	Fissurina staphylleana							1		
	Globobulimina spp						1		3	
	Globocassidulina oblonga							1	2	8
	Gyroidinoida lamarckiana				1		2	17	10	24
	Gyroidinoida soldanii							1		
	Hyalinea balthica			1	105	9	27	108	8	
	Lagena spp								2	2
	Lenticulina calcar								1	9
	Lenticulina sp				1					
	Melonis affinis				8	1	23	44	3	5
	Melonis pompilioides				8		9	15	9	10
	Neolenticulina variabilis									1
	Nonionella turgida									1
	Planulina ariminensis						20	45	13	35
	Pullenia quadriloba									6
	Robertina sp							1		
	Robertina translucens								1	1
	Saracenaria sp									3
	Siphogenerina columellaris									1
	Siphonina sp									1
	Sphaeroidina bulloides							2		2
	Stainforthia concava				3					
	Uvigerina mediterranea							12		1
	Uvigerina peregrina						4	3	6	7
	Valvulineria bradyana						13	2	11	1
porcelanous species	*Adelosina* sp							1		1
	Articulina tubulosa								1	2
	Biloculinella sp									11
	Comuloculina foliacea								2	
	Pyrgo depressa							1	2	2
	Pyrgo elongata							2		4
	Pyrgoella irregularis						1	2		
	Quinqueloculina padana						2	2	2	11
	Quinqueloculina stelligera						1	2		3
	Quinqueloculina sp								2	8
	Sigmoilopsis schlumbergeri				1		1	1	3	1
	Siphonaperta sp							1		
	Spiroloculina excavata								2	1
	Triloculina tricarinata							2		
	Triloculina sp								1	
	Textularia spp									2
	unidentified species			4	4	1		2	1	2
	total number of counted foraminifera	0	0	14	332	423	331	535	377	310
	total number of shallow water individuals	0	0	9	0	1	1	1	4	5
	total number of bathyal individuals	0	0	5	332	422	330	534	373	305
	BFN (bathyal species only, ind.g^{-1})	0	0	0	386	30	209	277	459	194
	S (number of bathyal taxa)	0	0	1	13	13	24	34	30	40

1442

Table SI2: Ecological assignment of main foraminiferal species in core CS22

Fontanier, F., Garnier, E., Brandily, C., Dennielou, B., Bichon, S., Gayet, N., Eugene, T., Rovere, M., Grémare, A., Deflandre, B. 2016. Living (stained) benthic foraminifera from the Mozambique Channel (eastern Africa): Exploring ecology of deep-sea unicellular meiofauna. Deep-Sea Research I 115, 159–174.

Species adapted to high oxygen conditions (HO)
Cibicidoides spp
Gyroidina lamarckiana
Miliolids excluding *Articulina tubulosa*
Low-oxygen indicators (LO)
Chilostomella spp
Globobulimina spp
Stainforthia concava
Species adapted to high organic fluxes (eutrophic indicators)
adapted to low oxygenation
Bolivina alata
Bolivina dilatata
Bolivina spathulata
not tolerant to low oxygenation
Bulimina marginata
Hyalinea balthica

(after Cornuault et al. 2016 and references therein; Fontanier et al. 2016)

Table SI3: Comparative list of taxa between the Marmara Sea (cores CS22 and CS18) and the SE Black Sea (core 22-GC3; Shumilovskikh et al., 2013).

	CS22	CS18	22-GC3	
	Pyxidinopsis psilata,	Pyxidinopsis psilata,	Pyxidinopsis psilata,	
	Spiniferites cruciformis/Galeacysta etrusca,	**Spiniferites cruciformis/Galeacysta etrusca,**		VV
		Galeacysta etrusca,		0
	S. cruciformis A,	S. cruciformis A,	S. cruciformis,	
	S. cruciformis B,	S. cruciformis B,	S. cruciformis,	
	S. cruciformis C,	S. cruciformis C,	S. cruciformis,	
		Pterocysta cruciformis,		0
	S. inaequalis,	**S. inaequalis,**		VV
		Romanodinium areolatum,		0
		Caspidinium rugosum,	Caspidinium rugosum,	
		C. rugosum rugosum,		only in MIS6
		Impagidinium sp. A,		only in MIS6
6/13		**I. caspienense,**		0
	Lingulodinium machaerophorum ss,	Lingulodinium machaerophorum ss,	Lingulodinium machaerophorum,	
		L. machaerophorum B,		0
1/3		**L. mach. bulbous,**		0
		Dubridinium caperatum,	Dubridinium caperatum,	
		Lejeunecysta marieae,		0
			Lejeunecysta sabrina?	0
			Quinquecuspis sp.	0
			Quinquecuspis concreta	VV
	Votadinium calvum,	Votadinium calvum,	Votadinium calvum,	
	Brown baggy cyst,	Brown baggy cyst,	Brigantedinium sp.	
			B. cariacoense	V
			B. simplex	V
			C. Gymnodinium microret./nolleri	0
	Xandarodinium xanthum,	Xandarodinium xanthum,	Xandarodinium xanthum,	
	C. Protoperidinium nudum,	C. Protoperidinium nudum,	C. Protoperidinium cf nudum	
		C. Protoperidinium stellatum,	C. Protoperidinium stellatum,	
	C. Polykrikos hartmanii,	**C. Polykrikos hartmanii,**		0
			C. Polykrikos schwartzii	0
			Echinidinium sp.	0
5/8			**E. zonneveldiae**	0
	S. belerius,	S. belerius,	S. belerius,	
	S. bentorii,	S. bentorii,	S. bentorii,	
			S. bulloideus	0
	S. elongatus,		S. elongatus,	
	S. hainanensis,			V
			S. hyperacanthus	VV
			S. membranaceus	VV
	S. ramosus,	S. ramosus,	S. ramosus,	
	S. septentrionalis,	S. septentrionalis,	S. septentrionalis,	
	Spiniferites sp.,	Spiniferites sp.,	Spiniferites sp.,	
	S. mirabilis,	S. mirabilis,	S. mirabilis,	
	S. pachydermus,		S. pachydermus,	
	Polysphaeridium zoharyi,	**Polysphaeridium zoharyi,**		VV
	Tuberculodinium vancampoae,	Tuberculodinium vancampoae,	Tuberculodinium vancampoae,	
	Operculodinium israelianum,	Operculodinium israelianum,		0
	O. centrocarpum,	O. centrocarpum,	O. centrocarpum,	
	Ataxodinium choane,	Ataxodinium choane,	Ataxodinium choane,	
	Bitectatodinium tepikiense,	Bitectatodinium tepikiense,	Bitectatodinium tepikiense,	
	Tectatodinium pellitum,	Tectatodinium pellitum,	Tectatodinium pellitum,	
	C. Pentapharsodinium dalei,	C. Pentapharsodinium dalei,	C. Pentapharsodinium dalei,	
		C. Alexandrium sp.,		0
	C. Scrippsiella trifida,	**C. Scrippsiella trifida,**		VV
	Pyxidinopsis reticulata,			0
21/17	Nematosphaeropsis labyrinthus,	Nematosphaeropsis labyrinthus,	Nematosphaeropsis labyrinthus,	
			Achomosphaera cf andalousiense	VV
	33	41		
				0 = insignificant
				V = different
				VV = very different

1455

1456